Anomaly General Circulation Models

A. NAVARRA

Geophysical Fluid Dynamics Program, Princeton University, Princeton, New Jersey

K. MIYAKODA

Geophysical Fluid Dynamics Laboratory/NOAA, Princeton University, Princeton, New Jersey

(Manuscript received 3 April 1987, in final form 15 December 1987)

ABSTRACT

Anomaly models based on a spectral general circulation model (GCM) are formulated and applied to a study of low-frequency atmospheric variability in the extratropics, and long-range forecasting research. A steady linear version of the anomaly model is treated by a matrix method. This model consists of nine vertical levels, 15 wave rhomboidal truncation, primitive equation system, and a fixed basic state, which is three-dimensionally variable. The matrix to be handled is extremely large, but can be solved using Krylov's technique. The solutions represent various teleconnection patterns known in the observed atmosphere. The sensitivity of the response of this anomaly model to zonal variability of the temporally fixed basic fields and to the geographical position of tropical heatings is investigated. The solutions of the steady linear anomaly model are compared with those of the original GCM, revealing that there are a few similarities among the solutions, but considerable discrepancies are also evident. A time-dependent nonlinear anomaly model is applied to further investigate the discrepancy. It appears that transient eddies are crucial for explaining the disagreement, although the study with the time-dependent anomaly model is preliminary.

A noteworthy aspect of the overall approach is that the anomaly models are derived, with only small modifications, from the full GCM, and therefore, their relationship can be readily investigated. It is concluded that the steady linear model may be used as a diagnostic tool for investigating the characteristics of the full GCM and the dynamics of a particular state of the atmosphere. However, caution is needed when there is a significant role played by transient eddies, and in the treatment of tropical Rayleigh friction.

1. Introduction

The Long-Range Numerical Weather Forecasting Group in Beijing, China (1977, 1979) and Chao et al. (1982) proposed an atmospheric–oceanic model that treats anomaly components, forced by the effect of SST (sea surface temperature). The equation for SST is solved numerically by integrating in time, whereas the equations for the atmospheric anomalies are assumed to be stationary. This model was applied to real cases and a number of monthly and seasonal forecasts were performed with some skill (see Chao et al. 1982; Miyakoda and Chao 1982). Opsteegh and Van den Dool (1980) also used a model that is based on a similar concept. Their model treats the departure from zonal mean instead of the anomaly from the zonally asymmetric climatology.

Originally the anomaly model was considered to be advantageous in avoiding two difficulties which are involved with the conventional time-dependent GCM, i.e., systematic error (climate drift) and complexities due to the nonlinearities. Hollingsworth et al. (1980), in a study of 10-day forecasts, showed that a large portion of error is contained in the planetary scale waves. Miyakoda et al. (1986) has concluded that a reasonable monthly forecast is possible only by eliminating a considerable amount of climate drift for the particular GCM. With respect to the anomaly model, observed information can be utilized for the basic state, thereby unburdening the forecast from carrying along the evolution of the basic climatic component. Besides, in the usual GCM it is extremely complicated to identify a clear-cut cause-and-effect relationship between external forcings or internal dynamics and the resulting solutions. With regard to the anomaly model, one can find straightforwardly the cause for a particular anomaly pattern by investigating anomalous boundary forcings, such as the soil moisture, the SST, or the anomalous atmospheric basic state. The steady linear (SL) anomaly model provides a precise single solution for the specified forcing or for the prescribed basic state.

However, a question is to what extent the solutions of the SL model have practical value, or to what extent they are associated with those of the nonlinear full

Corresponding author address: Dr. Kikuro Miyakoda, Geophysical Fluid Dynamics Laboratory/NOAA, Princeton University, P.O. Box 308, Princeton, NJ 08542.

GCM. Cubasch (1985) has recently published a provocative article, casting serious doubt on the capability of simple models to explain a number of atmospheric processes, including the teleconnection effect. It is true that the behavior of midlatitude atmospheric circulation is extremely complicated and that the variability even in the time averaged form is too subtle to be predicted accurately. We believe, however, that the stepwise relaxation of constraints from a simple model to a complex model is a good strategy for illuminating the complex mechanism (Hoskins 1983), and that the SL anomaly model constitutes an intermediate level of complexity.

Recently Geisler et al. (1985) have pointed out that the teleconnection patterns as revealed by their GCM are different from those of linear models. The GCM solutions are insensitive to the longitudinal positioning of the tropical thermal forcing, so far as remote responses are concerned. The postulated reason is that the midlatitude jet streams induce a secondary and yet dominant energy source for Rossby wavetrains associated with a kind of instability. This instability which was originally termed "normal mode instability" by Simmons et al. (1983) is related to the presence of a two-dimensionally-varying basic flow in a barotropic atmosphere. We will hereafter refer to the resulting disturbance as the SWB disturbance (Simmons–Wallace–Branstator) (Pierrehumbert, personal communication).

The SL anomaly model in this paper contains the SWB disturbance in a more generalized form, which includes baroclinic effects as well as the lateral wind shear of the basic flow. The combined baroclinic–barotropic instability was extensively investigated by Frederiksen (1982, 1983).

One of the thrusts in this paper is that anomaly models can be derived, without extensive changes to the conventional GCM. In other words, the anomaly GCM and the full GCM are closely linked, and therefore, this simple model may be useful as a diagnostic tool for the full GCM's simulation. The SL anomaly model, however, sometimes shows a considerable discrepancy from the full GCM, especially for the extratropical solution. It appears that, in addition to the SWB stationary distrubance, the transient eddies may play a significant role in forming teleconnection wavetrains. This issue will be addressed by use of a time-dependent nonlinear anomaly model.

2. Formulation of the anomaly model

The spectral "transform" model used here is based on the GCM of Gordon and Stern (1982). The relevant equations in the present discussion are: tendencies of vorticity, ζ; divergence, D; temperature, T; and surface pressure, p_s; as well as the hydrostatic equation. For the sake of discussion, the equation for the mixing ratio of water vapor, q, will be mentioned here, but it will not be used for the anomaly model in this paper.

a. Basic equations

Using a sigma ($\sigma = p/p_s$) vertical coordinate, and horizontal coordinates of the longitude, λ, and latitude, ϕ, the set of equations is written as

Vorticity:

$$\frac{\partial \zeta}{\partial t} = -\nabla \cdot \mathbf{k} \times \mathbf{s} + \mathbf{k} \cdot \nabla \times \mathbf{F}_2 \tag{2.1}$$

Divergence:

$$\frac{\partial D}{\partial t} = \nabla \cdot \mathbf{s} - \nabla^2\left(\phi + \frac{\mathbf{v} \cdot \mathbf{v}}{2}\right) + \nabla \cdot \mathbf{F}_2, \tag{2.2}$$

where

$$\mathbf{s} = -(\zeta + f)\mathbf{k} \times \mathbf{v} - \dot{\sigma}\frac{\partial \mathbf{v}}{\partial \sigma} - RT_v \nabla P \tag{2.3}$$

$$P = \ln p_s \tag{2.4}$$

Temperature:

$$\frac{\partial T}{\partial t} = -\nabla \cdot (\mathbf{v}T) + TD + \frac{RT}{c_p}\frac{\omega}{p} - \dot{\sigma}\frac{\partial T}{\partial \sigma} + \frac{Q}{c_p} + F_3 \tag{2.5}$$

Moisture:

$$\frac{\partial q}{\partial t} - \nabla \cdot (\mathbf{v}q) + qD - \dot{\sigma}\frac{\partial q}{\partial \sigma} - \frac{Q_2}{L} + F_4 \tag{2.6}$$

Surface pressure:

$$\frac{\partial P}{\partial t} = -\left(\int_0^1 \mathbf{v}\, d\sigma\right) \cdot \nabla P - \int_0^1 D\, d\sigma \tag{2.7}$$

Hydrostatic relation:

$$\frac{\partial \phi}{\partial \sigma} = -\frac{RT_v}{\sigma} \tag{2.8}$$

where $f = 2\Omega \sin\phi$ is the Coriolis parameter; $\mathbf{v}$ is the horizontal wind vector; $\dot{\sigma}$ is the vertical sigma velocity; ω is the vertical pressure velocity; ϕ is the geopotential height; R is the gas constant; c_p is the specific heat capacity at constant pressure; L is the latent heat of condensation; and T_v is the virtual temperature. Here, Q is a diabatic heating function, and is written as (Yanai et al. 1973)

$$Q = Q_1 + Q_R \tag{2.9}$$

where Q_R is the radiational heating; Q_1 is the "apparent heat source" due to the condensation; and Q_2 is the "apparent moisture source". In (2.2) $\mathbf{F}_2$ is the eddy viscosity vector, and F_3 and F_4 are the eddy thermal and moisture diffusion, respectively. All F terms include both horizontal and vertical diffusion.

b. Anomaly equations

All variables are now divided into two components, i.e., the climatological norm $(\ )_c$ and the deviation or

the anomaly $(\ )'$. The climatological norm is defined by arithmetic average of a variable over the whole sample. The norm is expressed by

$$(\ )_c = E(\ ), \tag{2.10}$$

where E denotes the ensemble mean. Using this notation, any variable is written as

$$\zeta = \zeta_c + \zeta' \tag{2.11}$$

$$F = F_c + F', \quad \text{etc.} \tag{2.12}$$

Inserting the split variables in Eq. (2.1), for example, and taking the ensemble mean of the equation, we have

$$\frac{\partial \zeta_c}{\partial t} = -\nabla \cdot \mathbf{k} \times \mathbf{S}_c + \mathbf{k} \cdot \nabla \times (\mathbf{F}_2)_c + \mathrm{Re}(\zeta_c) \tag{2.13}$$

where

$$\mathbf{S}_c = -(\zeta_c + f)\mathbf{k} \times \mathbf{V}_c - \dot{\sigma}_c \frac{\partial \mathbf{V}_c}{\partial \sigma} - R(T_v)_c \nabla P_c. \tag{2.14}$$

This is the equation for the climate part of vorticity. Subtraction of Eq. (2.13) from Eq. (2.1) leads to the equation for the anomaly part of vorticity, i.e.,

$$\frac{\partial \zeta'}{\partial t} = -\nabla \cdot \mathbf{k} \times \mathbf{S}^* + \mathbf{K} \cdot \nabla \times \mathbf{F}_2' - \mathrm{Re}(\zeta') \tag{2.15}$$

where

$$\begin{aligned} \mathbf{S}^* = &-(\zeta_c + f)\mathbf{k} \times \mathbf{v}' - \zeta' \mathbf{k} \times \mathbf{v}_c - \zeta' \mathbf{k} \times \mathbf{v}' \\ &- \dot{\sigma}_c \frac{\partial \mathbf{v}'}{\partial \sigma} - \dot{\sigma}' \frac{\partial \mathbf{v}_c}{\partial \sigma} - \dot{\sigma}' \frac{\partial \mathbf{v}_c'}{\partial \sigma} - R(T_v)_c \nabla P' \\ &- R(T_v)' \nabla P_c - R(T_v)' \nabla P'. \end{aligned} \tag{2.16}$$

These equations (2.13) and (2.15) include the term, Re, i.e., the second order correlation of the anomalies in the ensemble mean:

$$\begin{aligned} \mathrm{Re} &= -E(\nabla \cdot \mathbf{k} \times \mathbf{S}^*) \\ &= \mathrm{Re}(\zeta_c) \\ &= \mathrm{Re}(\zeta'). \end{aligned} \tag{2.17}$$

The Reynolds term, $\mathrm{Re}(\cdot)$, enters both the equation for the climate (2.13) and the anomaly (2.15) but with opposite signs. This symmetry is generated by the ensemble-mean splitting (2.11) or (2.12) when it is applied to the nonlinear terms. The Reynolds terms represent the interaction between the climate basic state and the anomaly component. Similar manipulations of Eq. (2.1)–(2.7) lead to the complete set of "Anomaly equations", for instance

$$\frac{\partial D'}{\partial t} = \cdots + \nabla \cdot \mathbf{F}_2' - \mathrm{Re}(D') \tag{2.18}$$

$$\frac{\partial T'}{\partial t} = \cdots + \frac{Q'}{c_p} + F_3' - \mathrm{Re}(T'). \tag{2.19}$$

The other equations are not written here.

In this system the equations of the climatological variables are not used, but the climatological norms are assumed to be known. They are fixed in time or are forced to vary slowly. This is a key aspect of the anomaly model. Another unique point is that the terms, Re, are involved in the equations. These terms are referred to in this paper as the Reynolds term, in analogy to the Reynolds stress terms that arise in turbulence theory.

c. *Lower boundary conditions*

The terms $\mathbf{F}_2$, F_3 and F_4 in Eqs. (2.1)–(2.6) represent the divergences of subgrid-scale eddy fluxes, which are required in spatially discretized or spectrally truncated models. These terms are divided into the horizontal and the vertical parts.

At the earth's surface, the turbulent fluxes are assumed to be governed by bulk aerodynamic drag laws, i.e.,

$$\tau_0 = -\rho C_D |\mathbf{v}| \mathbf{v} \tag{2.20}$$

$$H_0/C_p = -\rho C_D |\mathbf{v}| [\theta(z) - \theta(z_0)] \tag{2.21}$$

$$E_0 = -\rho C_D \beta |\mathbf{v}| [q(z) - q_{\mathrm{sat}}(T_s)] \tag{2.22}$$

where C_D is the drag coefficient; β the availability of soil (or sea) moistures; $q_{\mathrm{sat}}(T_s)$ the saturation value of q at the surface temperature T_s; z a level close to the earth's surface; and z_0 the roughness height.

There are nine vertical levels in the model atmosphere. Some of the variables such as ζ, D and T are specified at $k = 1, 2 \cdots 9$, and the vertical velocity σ is specified at $k = \frac{1}{2}, 1\frac{1}{2}, \cdots 9\frac{1}{2}$, where k is the index for the vertical levels, and the earth's surface corresponds to $k = 9\frac{1}{2}$.

In the horizontal directions, all variables are expressed in terms of spherical harmonic functions as

$$\begin{bmatrix} \zeta \\ D \\ T \\ P \\ q \end{bmatrix} = \sum_{m=-M}^{M} \sum_{n=|m|}^{|m|+J} \begin{bmatrix} \zeta_n^m \\ D_n^m \\ T_n^m \\ P_n^m \\ q_n^m \end{bmatrix} Y_{n,m}(\phi, \lambda) \tag{2.23}$$

where $Y_{n,m}$ is the spherical function defined by

$$Y_{n,m} = P_{n,m}(\phi) e^{im\lambda}, \tag{2.24}$$

$P_{n,m}$ is the Legendre function for planetary wavenumber n and zonal wavenumber m and M, J are the order of truncation. In practice, we use rhomboidal truncation, i.e., $M = J$; R15, for example, denotes rhomboidal truncation at the zonal wavenumber 15, i.e., $M = 15$. The anomaly equations can be treated using the same spectral transform technique used for the full GCM. In fact, simple, "surgical", changes can be made to the GCM code in order to transform it into an anomaly model.

3. Design of models

A four-model hierarchy is considered by combining three aspects of models' features, i.e., the total component versus the anomaly component, the time-dependent nonlinear (TN) versus the steady linear (SL) versions, and finally the inclusion or exclusion of moisture. Thus the models are: (i) the original total model; (ii) the simplified total model, in which the equations of moisture are not included, but the external parameters, Q' and T'_s are prescribed; (iii) the TN anomaly model; and (iv) the SL anomaly model. Heating functions are prescribed in the last three models. In this paper, our focus is on the SL anomaly model. Yet the comparison of four models may be useful in elucidating the character of the SL model.

The model proposed by a group of Chinese Long-range Forecasting (1977) corresponds to the SL anomaly model, though they included nonlinear terms. The Chinese Group (1977) and Monin (1972) advocated that the assumption of steadiness serves to filter out the short-term synoptic processes from the solutions. This statement comes from the notion that the objective of the anomaly model is to obtain the long wave or the planetary wave due to anomalous forcing, and that the transient components may not affect the determination of these long waves. A question is whether this hypothesis is valid and whether the SL anomaly model is sufficient to meet the requirements for long-range forecasts. Thus one objective of this paper is to investigate the validity of the SL model as a diagnostic tool.

a. Original (full) total model

The full R15 GCM (Gordon and Stern 1982) is the original total model. A set of "control runs" is performed using this model and from this data set the basic fields, i.e., the climatological norms and Reynolds terms, are derived.

b. Simplified total model

A simplification is made by the omission of moisture. Namely, the equations of moisture are not used, and instead, *the external forcings, Q and γH_0 are specified from the data of the original total GCM.*

In principle, all variables, and Q and γH_0, should be prepared continuously in time, but in practice, they were stored at 3 hour intervals. If everything is exactly the same, the solutions of the simplified model should agree with those of the control runs, i.e., the original total GCM. In this respect, the omission of moisture should not affect the final results, however, the interval at which forcings are saved and the computational method could cause discrepancies.

Several different formulations of the simplified model were tried to find the best trade-off between manageability of calculations and reproducibility of the full GCM solution. It was found that forcing the model with deep convective heating and surface fluxes every 3 hours yielded a reasonable similarity with the total GCM. Better results were possible, however, by prescribing the surface temperature rather than the heat flux. The final version of the simple total model was forced by convective heating and by prescribed surface temperature at 3 hour intervals. The bulk formulas (2.20)–(2.21) were then used to obtain the momentum and heat fluxes.

c. TN anomaly model

From Eqs. (2.15)–(2.19), the TN anomaly model may be rewritten in the following way.

$$\frac{\partial \zeta'}{\partial t} = -\nabla \cdot \mathbf{k} \times \mathbf{S}^* + \mathbf{k} \cdot \nabla \times \mathbf{F}'_2 - \mathrm{Re}(\zeta') \quad (3.1)$$

$$\frac{\partial T'}{\partial t} = -\nabla \cdot (\mathbf{v}T)' + (TD)' - \left(\dot{\sigma}\frac{\partial T}{\partial \sigma}\right)' + \frac{R}{c_{p\cdot p}}(T\omega)' - F'_3 - \mathrm{Re}(T') + \frac{Q'}{c_p}. \quad (3.2)$$

The equations for divergence, surface pressure and the hydrostatic relation are not written here.

For the basic fields, the climatological variables derived in the original or the simplified total GCM are used. The climatological norms are T_c, V_c, $\dot{\sigma}_c$, Q_c etc., as functions of λ, ϕ and σ. The external parameters, Q', and T'_s are also specified.

The spherical harmonic representation is applied to the anomaly GCM. The right-hand side of these equations consists of several terms. However, these terms are very similar to each other in their mathematical forms, and therefore, from the coding standpoint, the same harmonic calculation routine is applied to them repeatedly.

d. SL anomaly model

This model is derived from the TN amomaly model by eliminating the nonlinear terms, the Reynolds terms, and supressing the time-derivative terms.

In the stationary model the parameterization of fluxes of momentum and heat is not included. The surface drag is usually represented by a Rayleigh dissipation term; Newtonian cooling is also customarily added to represent a radiational effect. However, these dissipation terms seem to play an important role in mimicking the overall effect of neglected nonlinear terms in the SL model. They provide a crude parameterization of the transient term that is not used in this model. Large dissipations have also been introduced in zonally asymmetric models to account for a proper treatment of critical lines (Nigam et al. 1986). Since the anomaly model is zonally asymmetric a critical line can become a critical surface and the equations

are probably singular close to $\mathbf{V} = 0$. It is important to realize that both u and v are zero at the critical surface. In the real atmosphere this is a relatively rare event and it is doubtful that continuous critical surfaces exist. The presence of other terms in the basic state like the mean state divergence and vertical velocity might also alter the balance, reducing the role of critical lines or surfaces. A number of different formulations of dissipation inspired by previous experience with zonally symmetric models are used in the following to explore the characteristic behavior of the asymmetric model with respect to the dissipation formulation.

4. Numerical calculation of SL model

The spectral linearized equations of (3.1)–(3.2) are symbolically written as

$$\frac{d\mathbf{x}}{dt} + A \cdot \mathbf{x} = \mathbf{F} \tag{4.1}$$

where the vector $\mathbf{x}$ represents the unknowns as ζ', D', T' and P'; $\mathbf{F}$ represents the external forcings (i.e, Q' and $\gamma \cdot T_s'$); and the matrix $\mathbf{A}$ consists of the basic climatological variables $\mathbf{V}_c$, $\dot{\sigma}_c$, ζ_c, D_c, T_c, ϕ_c, q_c and P_c. The orographic effect is implicitly included in P_c.

a. Matrix **A**

As has been demonstrated by Hoskins and Karoly (1981), among others, the solutions of ζ', etc. are wavelike, reflecting teleconnection patterns (Horel and Wallace 1981; van Loon and Rogers 1981). This implies that the relaxation method does not work for solving this equation, but that the direct method using matrix inversion is required. Hoskins and Karoly (1981) showed that in order to calculate $\mathbf{A}$, the tendency equations (4.1) are used. Namely, setting $\mathbf{F} = 0$, we have

$$\frac{d\mathbf{x}}{dt} = -\mathbf{A} \cdot \mathbf{x} \tag{4.2}$$

where $x = (x_1, \cdots x_k \cdots x_N)$. Therefore, if one chooses a vector,

$$\mathbf{e}_k = (0, 0 \cdots 0, 1, 0 \cdots),$$

where $\mathbf{e}_k$ is the kth-column of the N-dimensional identity matrix, then

$$\frac{dx_j}{dt} = -A_{jk} \quad \text{for} \quad j = 1, \cdots L. \tag{4.3}$$

This means that the kth column of $\mathbf{A}$ is equal to the tendency vector $-dx_j/dt$. In this way, all elements of $\mathbf{A}$ are calculated. After obtaining $\mathbf{A}$, Eq. (4.2) is ready to be solved by multiplying the vector $\mathbf{F}$ by the inverse of A.

b. Solving the matrix

Linear models have been considered by a number of investigators, among others, Grose and Hoskins (1979), Held et al. (1983) and Nigam (1983). But the approach in this paper differs from previous investigations in treating deviations from the nonzonal mean basic state. Note, however, that nonzonal symmetry was already treated by Simmons et al. (1983) and Branstator (1983) for the barotropic model, and by Frederiksen (1979, 1982) for the 2-level baroclinic quasi-geostrophic model. The model described here handles the dynamical processes of the standing eddies superposed on the fixed basic planetary waves within the framework of 9-level primitive equations. In this system, a zonally symmetric critical line would not be a problem at all. There are always "westerly ducts" in the model atmosphere of the longitudinally-dependent basic state (Webster and Holton 1982).

In this general treatment, however, a notoriously formidable problem occurs; the matrix to be inverted is extremely large. The basic fields are functions of λ, ϕ and σ, and the spatial resolution is R15 and nine vertical levels (R15L9). Thus the vector $\mathbf{x}$, for example, contains a large number of degree of freedom. The vector $\mathbf{x}$ is written as

$$\begin{aligned}\mathbf{x} = [&(T_0^0)_1, (\zeta_1^0)_1, (D_1^0)_1, \\ &\cdots (T_n^0)_1, (\zeta_n^0)_1, (D_n^0)_1 \cdots \\ &\vdots \\ &(T_0^0)_9, (\zeta_1^0)_9, (D_1^0)_9, (P_1^0), \cdots \\ &(\mathrm{Re}T_1^1)_1, (\mathrm{Re}\zeta_1^1)_1, (\mathrm{Re}(iD_1^1))_1, \cdots \\ &\vdots \\ &(\mathrm{Im}T_1^1)_1, (\mathrm{Im}\zeta_1^1)_1, (\mathrm{Im}(iD_1^1))_1, \cdots]\end{aligned} \tag{4.4}$$

where Re and Im are the real and imaginary parts, respectively, and $(\zeta_n^m)_9$, for example, is the coefficient of order n and degree m at the vertical level 9. The total length of the vector is: $L = (2J + 1)(J + 1)(3k + 1) - (2J + 1)$ (see Navarra 1987). For a barotropic model (R15L1, $J = 15$, $k = 1$), L is 496; and for the nine vertical level baroclinic model (R15L9) L is 13 869. In the case of the zonally symmetric basic fields, the matrix $\mathbf{A}$ is block-diagonal, and the problem can then be split into inverting $J + 1$ submatrices, whereas, in the case of the zonally asymmetric basic fields, the full matrix has to be inverted simultaneously.

Thus the matrix contains a large number of components, and their distribution inside the matrix is dense without any special symmetry. In such a case, direct methods such as Gaussian elimination are not applicable. Navarra (1985, 1987) showed that a method using a Krylov subspace is effective for solving this problem numerically. The method (Saad 1981) is an iterative technique that uses a Galerkin condition to project the original problem on a smaller subspace. The Krylov subspace provides a much smaller matrix ($L = 1000$, for example) than the original one ($L = 13\,869$), and the smaller matrix is inverted at each iteration.

5. Characteristic of SL model solutions

a. Lateral friction

For the terms of lateral diffusion represented by $\mathbf{F}'_2$ and $\mathbf{F}'_3$ in Eqs. (3.1) and (3.2), three forms of friction/diffusion are employed. These forms are the biharmonic diffusion, Rayleigh damping for momentum, and Newtonian cooling for heat, i.e.,

$$F'_2 = K_m \nabla^4 \mathbf{v}' - \epsilon_m \mathbf{v}' \tag{5.1}$$

$$F'_3 = K_h \nabla^4 T' - \epsilon_h T'. \tag{5.2}$$

In the linear system, it appears crucial to incorporate adequate Rayleigh damping ϵ_m in the tropics, for the purpose of simulating the neglected nonlinearities. The discussions on friction formulation and the sensitivity of the results to the Rayleigh friction have been given by Simmons (1982), Nigam et al. (1986) and others. In fact, our study indicates that the model's solution is, to some extent, sensitive to the tropical specification of ϵ_m.

In the subsequent discussions, we will use three kinds of lateral frictions.

b. Friction A

The Rayleigh damping described herein was developed by Nigam et al. (1986); they applied this formulation successfully to the reproduction of the GCM simulation.

$$\epsilon_m = \max(\epsilon_b, \epsilon_c) \tag{5.3}$$

where

$$\epsilon_c = \left\{1.5 \exp\left[\left(\frac{u}{\sigma \cdot \cos\phi}\right)^2\right]\right\}^{-1} \text{ day}^{-1} \tag{5.4}$$

$$\epsilon_b = \begin{cases} [0.2/(\sigma - 0.8)]^{-1} \text{ day}^{-1}, & 0.8 < \sigma < 1.0 \\ 1000^{-1} \text{ day}^{-1}, & \sigma \leqslant 0.8 \end{cases} \tag{5.5}$$

σ being the vertical coordinate, and u the zonal mean of zonal wind in m s^{-1}. This Rayleigh friction is strong ($1 \sim 3$ day) in tropics, as well as near the surface, but weak (>100 day) in the middle latitudes. On the other hand, Newtonian cooling is

$$\epsilon_h = 0. \tag{5.6}$$

The biharmonic diffusion coefficients are

$$K_m = K_h = 5.0 \times 10^{16} \text{ m}^4 \text{ s}^{-1}. \tag{5.7}$$

c. Friction B

This Rayleigh friction is a simplified version of friction A. For $25°\text{N} \geqslant \phi \geqslant 25°\text{S}$ and all vertical levels

$$\epsilon_m = (1 \text{ day})^{-1}. \tag{5.8}$$

For the extratropics, i.e., $\phi \geqslant 25°\text{N}$ or $25°\text{S} \geqslant \phi$.

$$\epsilon_m(k) = \begin{cases} [60 - 59/8(k-1)]^{-1} \text{ day}^{-1}, \\ \quad \text{for} \quad k = 1, 2 \cdots 6 \\ 3^{-1} \text{ day}^{-1}, \quad k = 7 \\ 2^{-1} \text{ day}^{-1}, \quad k = 8 \\ 1 \text{ day}^{-1}, \quad k = 9, \end{cases} \tag{5.9}$$

k being the index of vertical level.

For all ϕ and for any k

$$\epsilon_h(k) = [10 - 5/8(k-1)]^{-1} \text{ day}^{-1} \tag{5.10}$$

$$K_m = K_h = 5.0 \times 10^{16} \text{ m}^4 \text{ s}^{-1}. \tag{5.11}$$

d. Friction C

For all latitudes

$$\epsilon_m(k) = \epsilon_h(k) = \begin{cases} [60 - 59/8(k-1)]^{-1} \text{ day}^{-1}, \\ \quad k = 1, 2, \cdots 6 \\ 3^{-1} \text{ day}^{-1}, \quad k = 7 \\ 2^{-1} \text{ day}^{-1}, \quad k = 8 \\ 1 \text{ day}^{-1}, \quad k = 9 \end{cases} \tag{5.12}$$

$$K_m = K_h = 15.0 \times 10^{16} \text{ m}^4 \text{ s}^{-1}. \tag{5.13}$$

The values for K_m and K_h in the original GCM or the simplified total model, are 1.0×10^{16} m^4 s^{-1}, which corresponds to a decay rate of (150 day)$^{-1}$ for planetary wavenumber 10. Friction A and C use 5 and 15 times larger values. The magnitude of K_m and K_h does not seriously affect the resulting flow pattern but they influence the convergence rate appreciably. Friction A represents weakest damping; and Friction C the strongest damping.

e. Example

Figures 2 and 3 display preliminary results of the anomaly model from a January 1983 case using a reduced resolution model. A particular heating function Q' in Fig. 1 is similar to the one used in theoretical studies of Webster (1972), Gill (1980), and Lim and Chang (1983), but it is slightly different; the positive as well as negative values are juxtaposed. When a positive SST anomaly emerges at a certain location in the equatorial zone, a negative SST anomaly often appears next to the region (see Keshavamurti 1982; Shukla and Wallace 1983). In this case, the node of this heating dipole is located at the dateline. The vertical distribution is sinusoidal with zero at the bottom and the top of the model atmosphere. It, therefore, represents internal heating in the definition of Lim and Chang (1983). The maximum is at $\sigma = 0.5$, and its value is 10.0 mm d^{-1} in units of rainfall rate. This value was suggested by Arkin (1984); 14.0 mm d^{-1} is the maxi-

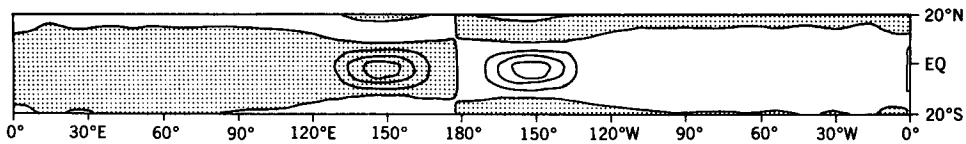

FIG. 1. Dipole heating Q'. The maximum corresponds to 10 mm d^{-1} in units of rainfall rate.

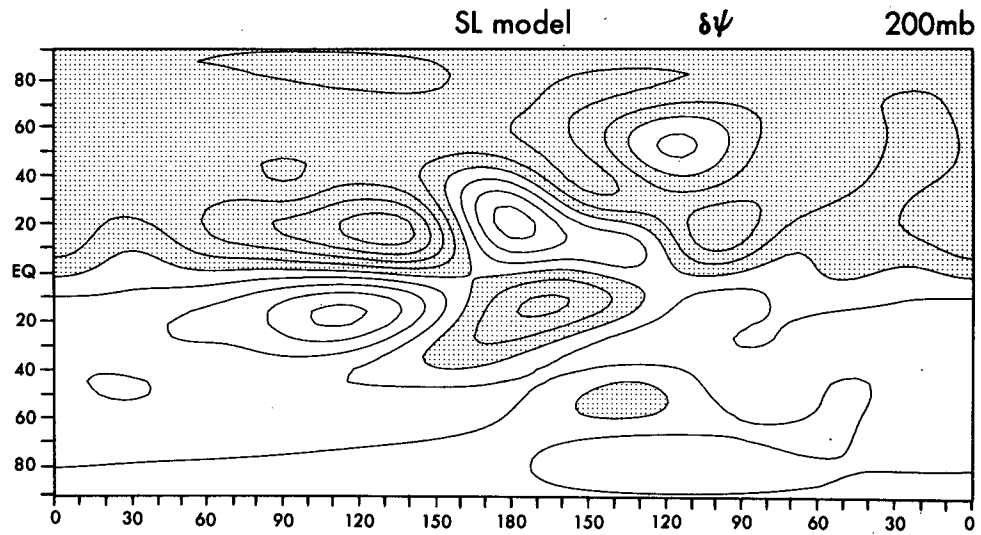

FIG. 2. Anomaly streamfunction, $\delta\psi$, obtained by the SL model with the dipole heating in Fig. 1, the node of which is at the dateline and the equator. Negative values are stippled. Contour interval is 1×10^6 m^2 s^{-1}.

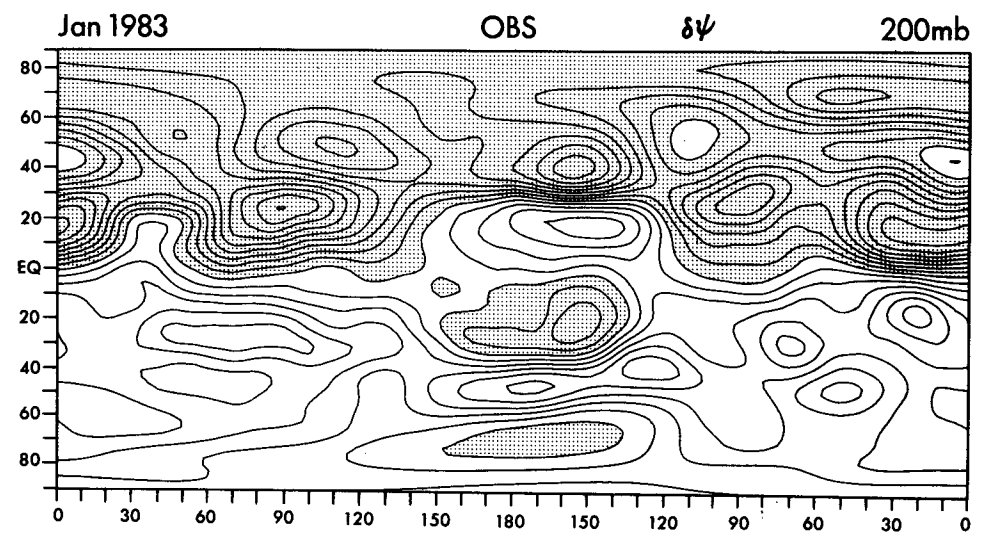

FIG. 3. Observed distribution of anomaly streamfunction for 10–30 January 1983. Negative values are stippled. Contour interval is 5×10^6 m^2 s^{-1}.

mum rate of rainfall derived from the anomaly of the outgoing longwave radiation, i.e., -80 W m^{-2} in the case of January 1983. This value is one of the largest realistic monthly mean precipitation rates one can expect.

Applying this anomaly heating, Q', the SL model at R7L9 resolution (low resolution is used only in Fig. 2) with Friction C was solved with the climatological basic fields (zonally varying). Figure 2 is the anomaly streamfunctions from the SL model, and Fig. 3 is the

observed map for January 1983, the anomaly streamfunction $\delta\psi$ being defined by $\nabla^2\delta\psi = \zeta'$. Surprisingly, the solution of $\delta\psi$ in the SL model closely resembles the observed anomaly streamfunction, though the intensities of the circulation are quite weak (note the different contour intervals in Figs. 2 and 3). The atmospheric response in the tropics to this heating is similar to those described by Gill (1980) and Lim and Chang (1983). The basic configurations of Kelvin and Rossby waves in the equatorial zone and the dynamics of waves were discussed by Matsuno (1966) and Webster (1972). A difference from Gill and Matsuno may be found in the teleconnection wave-train on the global scale. Despite internal forcings, these deep heatings appear to be capable of exciting external Rossby waves, probably due to the effect of vertical wind shear (Kasahara and Da Silvia Dias 1986); the waves propagate poleward in the westerly basic wind field (Egger 1977; Webster 1982). The distinct horizontal tilt of this wavetrain is reminiscent of the barotropic Rossby mode obtained by Lim and Chang (1983), and Lau and Lim (1984); and the vertical structure agrees with the external Rossby mode outside the tropics shown by Held et al. (1985). The teleconnection ray originating from the tropics has been revitalized in the baroclinic (Grose et al. 1984) and the horizontal shear instability zones in the midlatitudes, and has been modulated by the orographic effect (Kinter 1983). A comparison with a zonally symmetric solution for this case (not shown) indicates that there is less penetration of the forced waves in midlatitudes. Navarra (1985) showed that in a zonally varying basic state, disturbances originating in the tropics can be amplified in the jet zone, resulting in longer and stronger anomaly waves than in the zonally symmetric case. Friction eventually will dissipate the wave, but the zonally varying case is damped out at a slower rate. A question is whether the good agreement in Figs. 2 and 3 (in phase but not in amplitude) is a fortuitous coincidence or a logical consequence.

f. Effect of nonzonally symmetric basic state

The SL model for the same heating with Friction C is solved for two versions; one is with the climatological basic state, which is zonally varying, and the other is with the zonal mean basic state. Therefore, the former model includes stationary eddies in the fixed basic state, whereas the latter does not, and the solution in the former version may exhibit the strong SWB disturbance, whereas the latter does not. The zonal mean basic state in the latter mode is obtained by computing the zonal average of the basic state variables, i.e., U_c, V_c, T_c, σ_c and ω_c on σ-surfaces, in the former model, and thereafter replacing the basic state in the former model by these zonal means of the respective climatological variables. It is noted, however, that for $P_c(=(\ln p_x)_c)$ the original climatological distribution (i.e., longitudinally varying) is used in order to retain the same orographic effect.

Let us first look at Figs. 4a and 4b and Figs. 5a and 5b, in which the anomaly height patterns at 300 mb, δz, are shown for the case of 180° heating. The presentation consists of two kinds of maps. One is the longitude–latitude map, intended to show the near-field feature, and the other is the stereographic projection map for the far-field features. It is quite clear in these figures that the teleconnection patterns with the climatological basic state are considerably different from those with the zonal mean basic state. Figures 4a and 5a closely resemble propagating Rossby wavetrains along a near-great circle on a sphere from the equatorial region (Hoskins and Karoly 1981). Figures 4b and 5b depict complicated wavy patterns, that might be related to the two major energy centers identified in the zonally varying climatology (Branstator 1985; Navarra 1985). The equatorial waves appear amplified in the vicinity of the jet over Japan and, less appreciably for the North American Jet.

In summary, the stationary anomaly model has been shown to be feasible. Results indicate some capability of simulating equatorial forced flows. It also exhibits marked differences with the zonally symmetric case. The zonally asymmetric model exhibits a richer and more complicated behavior, with amplification of the signal away from the source in the jet regions.

6. Outline of experiments

a. Four steps

In order to explore the usefulness of the anomaly model, a more exact evaluation of the relationship between the SL anomaly model and the total GCM is attempted. For this purpose, four steps are taken corresponding to the four hierarchial models in section 3, as follows.

Step 1: Using the original total GCM and climatological values of SST, two month forecasts are performed for a number of January cases.

Step 2: Using the simplified total GCM and applying Q and T_s (every three hours) as obtained in Step 1, two month forecasts are carried out again for the same number of January cases as in Step 1. The initial conditions are the same as before. However, Step 2 includes two forecasts, i.e., one with $Q' = 0$ and the other with $Q' \neq 0$, the dipole heating as in Fig. 1.

Step 3: The SL anomaly model is solved with $Q' \neq 0$. This is the main part of this paper. SL has a zonally varying basic state.

Step 4: The TN model is solved with $Q' \neq 0$. This is done only for the purpose of understanding the role of transient eddies.

By its own nature, the SL solution in Step 3 is a result of only one integration for each case. On the other hand, the TN solution in Step 4, in principle, requires stochastic forecasts. However, the TN model study in this paper is preliminary; the initial conditions are based on the SL solution obtained in Step 3 for

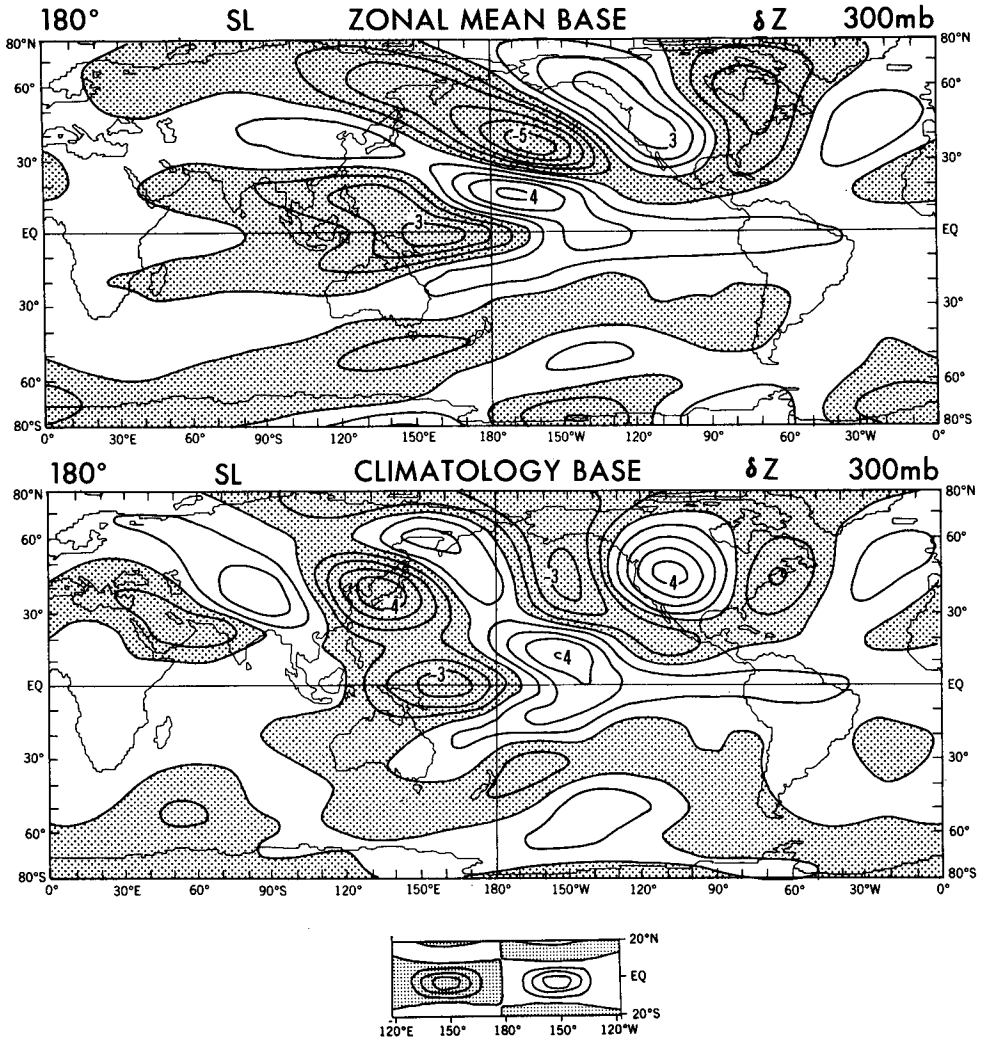

FIG. 4. 300 mb geopotential height anomalies in the SL models of the zonally symmetric basic field (upper) and of the climatological basic field (lower). The heat source, located at the equator and 180° longitude, is shown at the bottom. Contour interval is 100 m. Negative anomalies are shaded.

each case. Some additional runs were made by perturbing these initial conditions with random numbers. The overall results are not changed, as long as the magnitude of the perturbations remain small. The numerical results shown here are the ones obtained from the original nonperturbed initial conditions.

b. *Data samples and cases of heating locations*

The data samples are for 1 January 1977, 78, 79, 80, 81, 82, 83 and 16 January 1979. The initial conditions are based on the NMC (National Meteorological Center) analysis for 0000 UTC (see Miyakoda et al. 1986).

Three cases of equatorial heating $Q' \neq 0$ are treated, in a similar way to the study of Keshavamurti (1982). The nodes of the heatings are located at 120°E, 180°, and 120°W in the equatorial Pacific, and the intensities are the same as in Fig. 1.

c. *The simplified total GCM*

The approach with the GCM in Step 2 is similar to that of Blackmon et al. (1983) and Geisler et al. (1985) in many respects. The models employed in all these studies were spectral models with R15L9 resolution. The differences are listed in Table 1.

In Step 2, the difference between the solutions $Q' = 0$ and $Q' \neq 0$ is defined here as the "anomaly"; the height anomaly is written as

$$\delta z = Z(Q' \neq 0) - Z(Q' = 0). \qquad (5.1)$$

The simplified total GCM solutions maps for Step 2, shown in the lower parts of Figs. 6–8 and Fig. 9, are

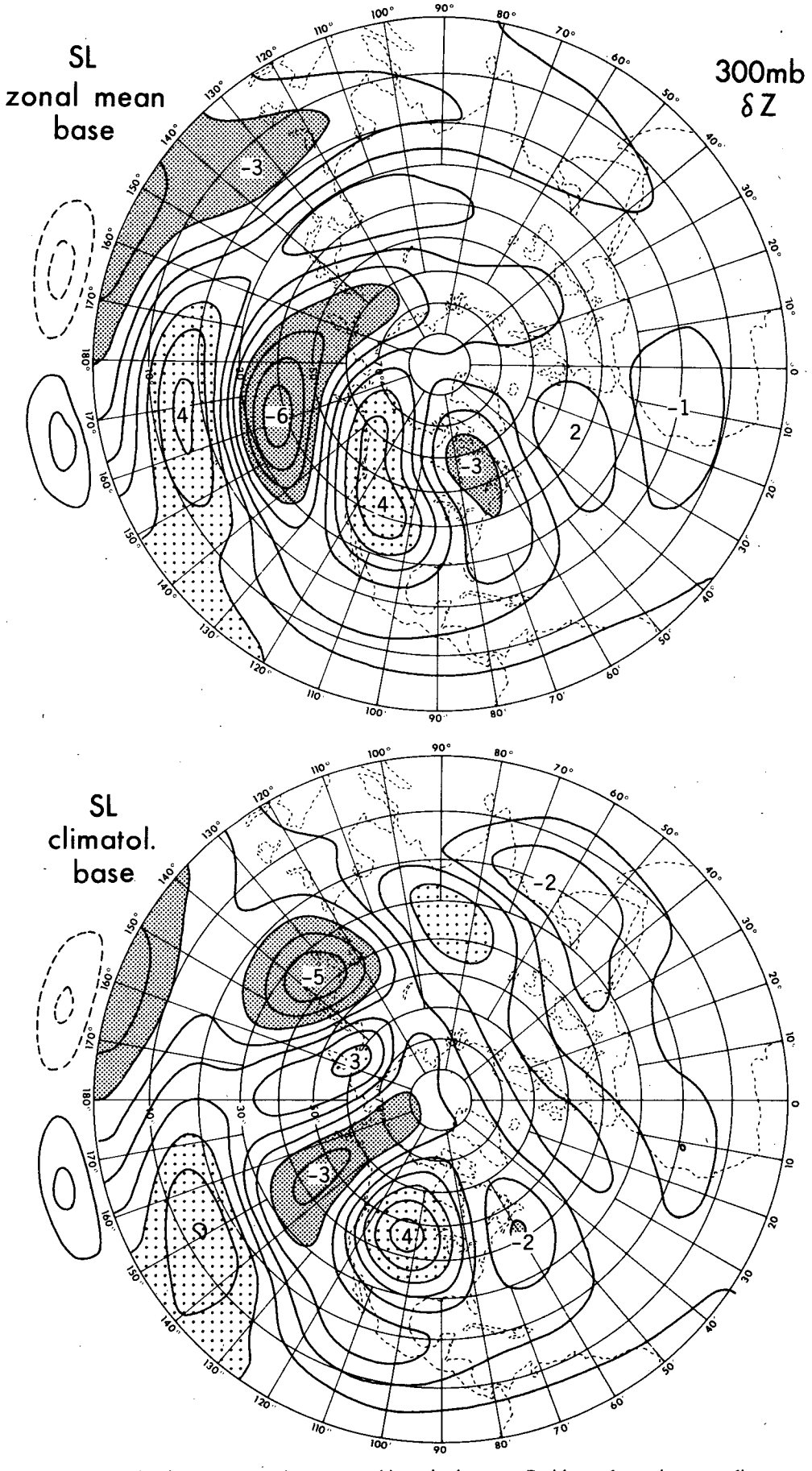

FIG. 5. As in Fig. 4 except on the stereographic projection map. Positive and negative anomalies are shaded in different ways.

TABLE 1. Spectral models with R15L9 resolution.

	Blackmon et al.; Geisler et al.	The present study
Model	Full GCM (Step 1 approach)	Simplified GCM (Step 2 approach)
Samples	8 realizations from model's perpetual Januarys	8 different real Januarys
Duration of run	90 days	60 days
External forcings	Anomaly of SST	Anomaly of heating
Anomaly heatings	8.7 mm day^{-1} predicted	10 mm day^{-1} specified
Longitudinal positions of equatorial heatings	2W 165°W (165°E)	120°E
	EPAC 120°W (150°W)	180°
	FAR 105°W (135°W)	120°W
	EPAC (max (node) SST anom)	

the arithmetic means over eight January samples, and also the time means for 30 days from 30 to 60 days (i.e., February). In the total GCM solutions, the disturbances in the extreme far fields should be small due to cancellation within eight samples, but in practice it did not happen.

These patterns of total GCM solutions are similar to those of Blackmon et al. (1983). In addition, Fig. 7b resembles the PNA (Pacific/North American) pattern, but to a lesser extent, as compared with Blackmon et al. The anticyclone pair anomaly around the equator in the tropical upper layer is less pronounced than Keshavamurti or Geisler et al.

In order to confirm the similarities among the GCM solutions for three different heatings, (Geisler et al. 1985) the correlation coefficients are calculated for the geopotential height and zonal wind anomaly patterns. Figures 10 and 11 show the vertical distributions of correlation coefficients for a pair of different tropical heatings, i.e., between 120°W and 180°, between 180° and 120°E, and between 120°E and 120°W. The verification domains are the tropics (25°N–25°S) and the extratropics (90°–25°N), the longitudinal sector being from 60°E through 180° to 30°W. The domain on which correlations are calculated has been chosen so as to contain most of the response to the tropical heatings, without having the adverse effect of including areas where the response is very small. The correlation coefficients were computed on a 2.5 × 2.5 deg grid. About 3700 grid points were used for the midlatitude domain, whereas 2900 points went into the calculation for the tropical domain.

Though some caution is in order in evaluating correlation coefficients, the diagrams are consistent with the visual inspection of the GCM solution patterns. The anomalies tend to be close to each other in the extratropics, as in Geisler et al. In the tropics, the correlation are low because of the phase shifts in the anomaly heating centers at the equator. The GCM response to the heating can then be divided into two parts, a local equatorial response, locked in phase to the heating, and a midlatitude response, phase-independent with regard to the heating location.

d. *Teleconnection indices*

The formulas of the teleconnection indices for the PNA are given by (Wallace and Gutzler 1981),

$$\text{PNA index} = \tfrac{1}{4}(\delta z^*_A - \delta z^*_B + \delta z^*_C - \delta z^*_D) \quad (5.2)$$

where δz^* is the normalized 500 mb height anomaly, defined by $\delta z/\langle(\ )^2\rangle^{1/2}$; δz are obtained from the SL (for TN) models; δz_{obs} are based on the NMC analyses; the ensemble average $\langle\ \rangle$ is performed with respect to a 30 year series of data, and the geographical positions for the point label are: A (20°N, 160°W), B (45°N, 165°W), C (55°N, 115°W) and D (30°N, 85°W).

Table 2 shows results of the teleconnection indices for the total GCM in Step 2 (multiplied by 100). The indices depend not only on the external forcing, but also on the initial condition. Perhaps it is important to note that the indices for all heating cases in this experiment show large positive values. For 120°W and 180° cases in particular, positive values are distributed homogeneously throughout the eight samples, only for one instance in each case is the index negative (see Geisler et al. 1985), while the PNA indices for the 120°E case diverge largely from one January sample to another, including negative values in many samples.

In their sensitivity study, Geisler et al. reported that the response generally consists of a well-defined PNA pattern, though the probability of exciting the PNA patterns decreases eastward from 165°E. The latter point is not evident in the result of this paper.

The Keshavamurti's study on the impact of three anomalous forcings in the equatorial Pacific concludes that the strengthening of the jet off Alaska is always observed in all three cases, and that this effect is smallest for forcing in the western Pacific, and strongest for forcing in the central Pacific. In these experiments, the numerical simulation of the 45°N, 165°W cyclone cell in the PNA wave train was not impressive and accordingly, the strengthening of the jet was not pronounced for three different cases of heating (see the lower parts of Figs. 6–8).

e. *Summary of this section*

The results of the GCM in Step 2 are consistent overall with those obtained by Geisler et al. (1985) or

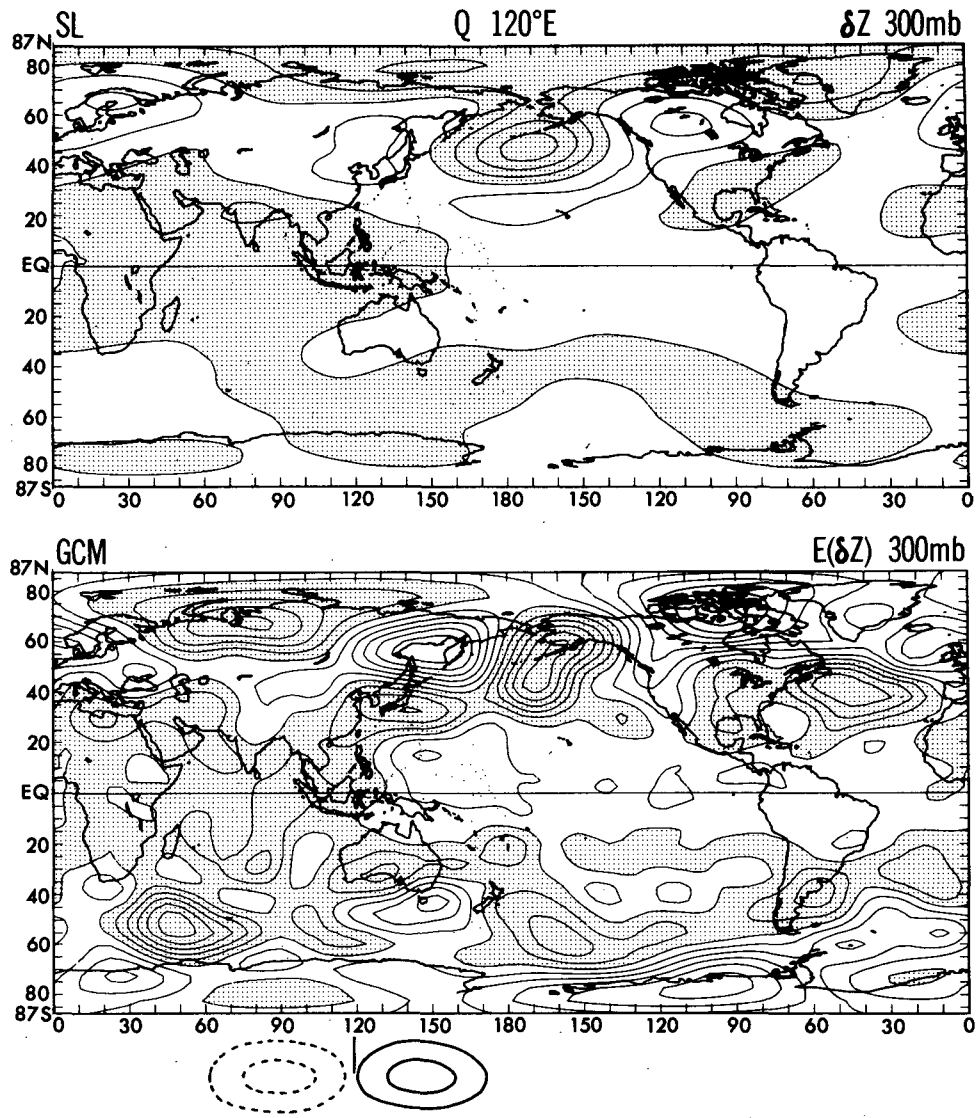

FIG. 6. Comparison of the solutions of the SL anomaly (upper) and of simplified total GCM (lower) in terms of the 300 mb geopotential height anomalies. The node of heat source is located at the equator and 120°E longitude. Contour interval is 200 m. Negative anomalies are shaded.

Keshavamurti (1982). *Irrespective of the locations of equatorial heat source, the teleconnection wave trains in the extratropics are similar to each other;* positive PNA patterns are present in all ensemble means for the respective heatings.

7. Solutions of SL model

The SL anomaly model in Step 3 with Friction A is applied to three cases of equatorial heatings. The upper parts of Figs. 6–8 display the 300 mb height anomaly patterns from Step 3. They are compared with the patterns of Step 2 in the lower parts of the figures, the contour intervals being the same both in the Step 2 and Step 3 patterns. A similar comparison is shown in Fig. 9 where the 300 mb geopotential height is mapped on a stereographic projection.

It may be said that the case of 120°E heating shows a certain degree of correspondence in the teleconnection patterns between Step 3 and Step 2 for the extratropics, while for the cases of 180° and 120°W heatings, there is no agreement. This feature may be shown more quantitatively in Figs. 10–13, which display vertical distributions of correlation coefficients for height and wind anomaly patterns between the Step 3 and Step 2 solutions. They are presented for both the tropics (25°N–25°S) and the extratropics (90°–25°N). The verification domains are different for various heating cases, i.e.; the longitudinal sections, 60°E–150°W for the 120°E heating case; 120°E–90°W for 180° heating cases; and 180°–30°W for 120°W heating cases.

The diagrams reveal that (i) the correlations in the extratropics are positive only in the case of 120°E

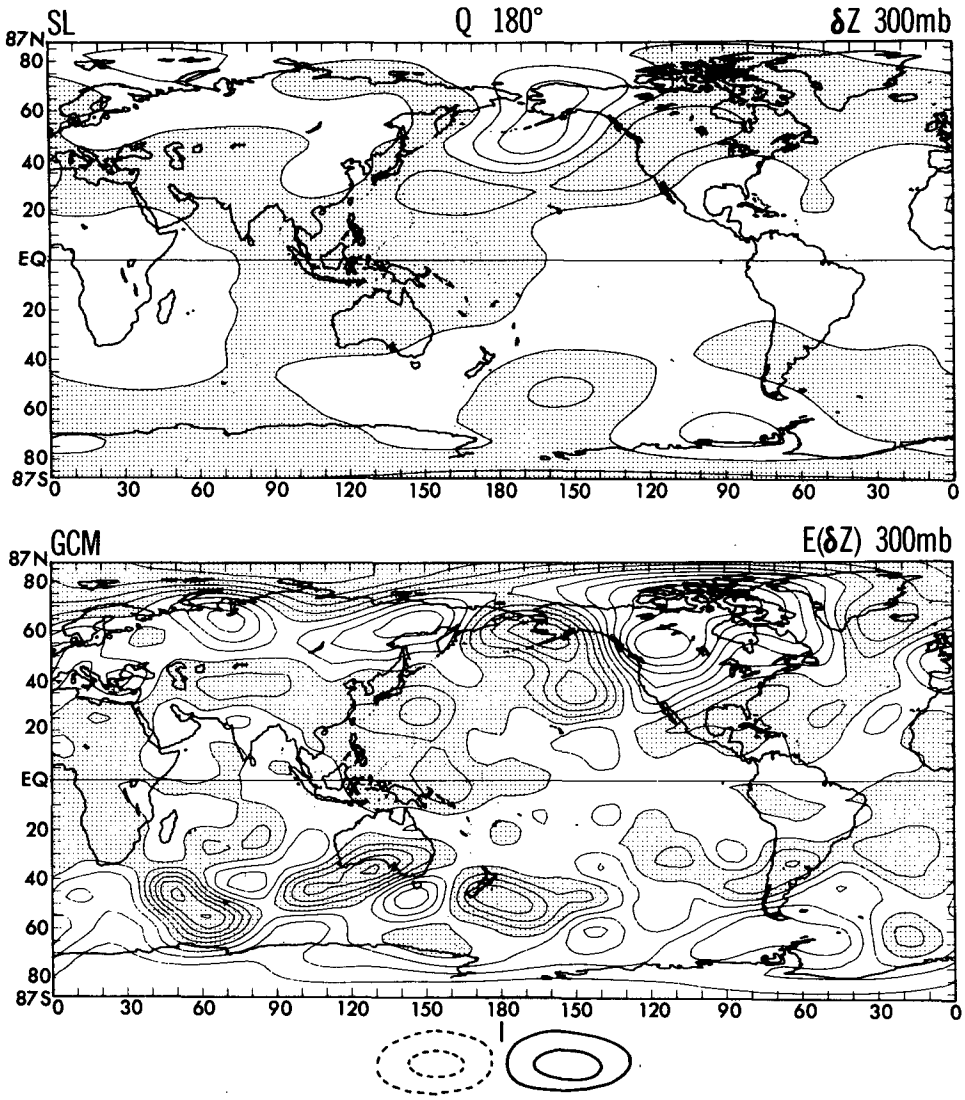

FIG. 7. As in Fig. 6 except that the node of the equatorial heat source is located at 180° longitude.

heating, and are negative for other heating cases; (ii) the correlations in the tropics have two modes in the vertical, reflecting the baroclinic circulation structure in the near field of the equatorial heating; (iii) the correlations in the tropics are high for all cases except near the node level and in the stratosphere; and (iv) the correlation curves in the extratropics appear monotonic in the vertical, compared with those in the tropics, reflecting the equivalent barotropic structure of wave trains in the far field from the source regions (Held et al. 1984; Opsteegh and Vernekar 1982).

Table 3 displays the PNA indices for the SL (and TN later) model solutions in Step 3 (and Step 4 later). In the absence of a comprehensive study of the SL model sensitivity to the different specifications of the basic state, climatology was chosen for the first experiment. It is of course conceivable that the solution will exhibit some sensitivity with respect to the basic state, but we will not go further into this topic in this paper. The basic state data were obtained from a Crutcher and Meserve (1970) compilation and it contains the full tridimensional structure of the stationary waves. The first row is the indices for the SL with Friction A.

Inspection of these indices for the SL models, together with Table 2, may lead to the following. First, the PNA indices in Table 3 agree with those in Table 2 only for the case of the 120°E heating. The indices for the 180° and 120°W heatings are negative, implying once again that there is a considerable discrepancy in the phase of teleconnection patterns.

To summarize this section, *the SL model with zonally asymmetric basic flow (Step 3) alone is unable to explain the whole teleconnection pattern of the PNA.* In particular, the fact that the anomalies in the Pacific/North American sector are similar irrespective of the longitudinal positions of equatorial heating cannot be

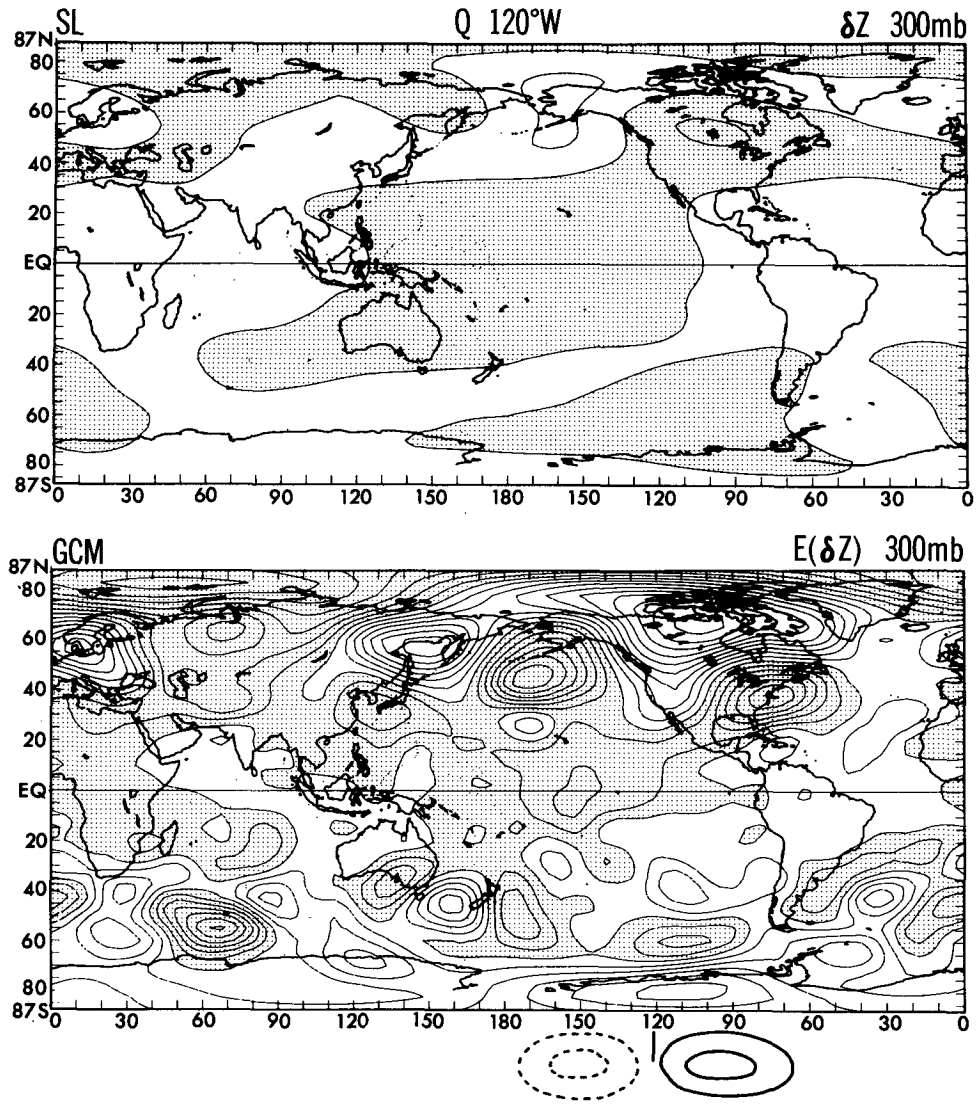

FIG. 8. As in Fig. 6 except that the node of the equatorial heat source is located at 120°W longitude.

reproduced. Although the results are not shown in this paper, the teleconnection patterns in the extratropics are affected by the specification of Rayleigh damping in the tropics with the framework of the SL anomaly model.

8. Remarks with TN anomaly model solutions

In order to examine the reason for the discrepancy of solutions between Step 3 and Step 2, we proceed to Step 4, i.e., the TN anomaly model. This model should provide the effect of transient eddies and nonlinearity.

The anomaly model system is represented by equations (3.1)–(3.5). The lateral diffusions in Eqs. (4.5)–(4.8) do not include Rayleigh damping, nor Newtonian cooling. Concerning the biharmonic diffusion coefficients and Reynolds terms, two versions are used.

Version I:

Reynolds terms, and $K_m = K_h = 5 \times 10^{16}$ m^4 s^{-1} (8.1)

Version II:

No Reynolds term, and

$$K_m = K_h = 20 \times 10^{16} \text{ m}^4 \text{ s}^{-1}. \quad (8.2)$$

In Version I, the Reynolds terms were calculated from the eight January cases based on the full GCM in Step 1. These terms are constant in time, but are functions of three-dimensional space. Vertical diffusion and anomaly surface turbulent fluxes were excluded.

Three numerical experiments were performed. Each experiment was designed to check the effect of nonlinearities and time-evolution for a particular equatorial

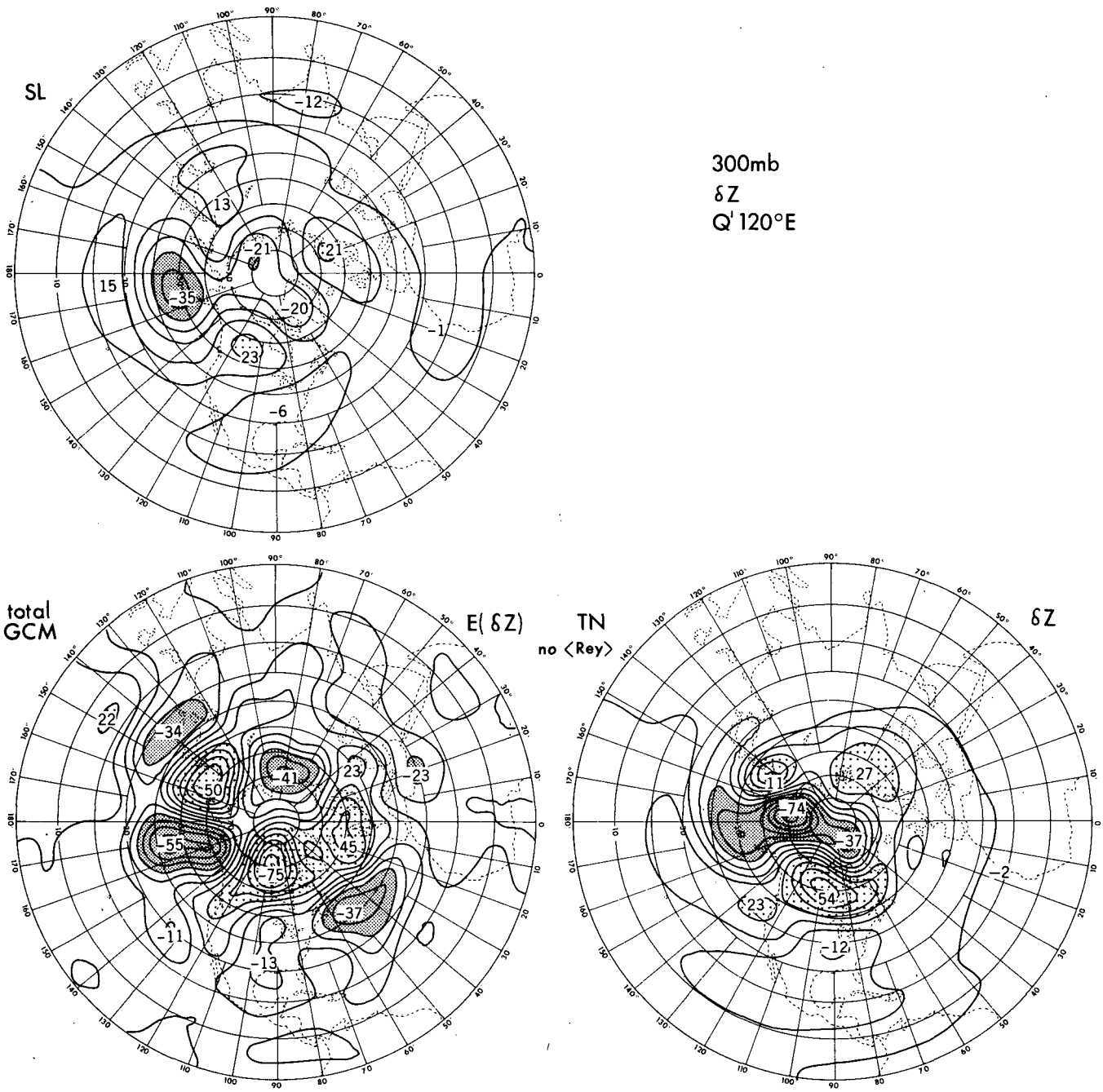

FIG. 9. Comparison of the geopotential height anomalies at 300 mb level for the three models for the heating node at 120°E. The SL anomaly model (upper left), the simplified total GCM (lower left), and the TN anomaly model (lower right). Contour interval is 200 m. The result of the TN anomaly model is the monthly mean for days 61–90. The model does not include ⟨Re⟩ term.

anomaly heating. In order to avoid the necessity of stochastic realizations, the initial condition for each case was chosen to be the solution of the SL model (with climatological basic state) corresponding to that heating, although, as mentioned earlier, the additional runs were made by slightly different initial conditions. The three experiments are not forecasts in a conventional sense; nevertheless they give some information on the nature of the nonlinear time evolution of the anomaly waves. In fact, if the initial conditions were the same as those used in the conventional forecasts, the TN model experiments would become exactly the same as the GCM run in Step 2.

The results of Step 4 with Version II are shown in Fig. 14 and Fig. 9. The solutions shown are the 30 day average for the third month. It may be noted that (1)

TABLE 2. Teleconnection indices (normalized) for GCM PNA indices (×100) Day 30–60.

Run	Years	120°E	180°	120°W
1	1977	3	8	14
2	1978	−5	−48	31
3	1979	1	41	57
4	16/79	−1	35	33
5	1980	89	78	42
6	1981	−8	33	−28
7	1982	−16	51	64
8	1983	124	81	152
Averaged pattern		23	35	46

the amplitudes are considerably increased, and (2) the flow patterns for the three heating cases start to resemble each other.

Figure 15 and 16 display the correlation coefficients between the TN anomaly (Step 4) and the simplified total GCM solutions (Step 2). It may be seen that the positive correlations are more dominant in the TN model case than in the SL model case, particularly for the extratropics. Comparing Fig. 16 and Fig. 13, it is possible to see that there is a trend toward more positive correlations in the TN integrations than in the SL case. The trend is more apparent in the extratropics than in the tropics. A similar analysis performed on the second month of the TN data yielded less satisfactory results. This may indicate that there is a tendency towards larger correlations (i.e., better agreement with the full GCM) as the integrations proceed. However, in this first study the TN integrations were stopped after three months. The results of Version I are similar to those of Version II, and Rayleigh terms slow down the speed of adjustment to the equilibrium state.

Observations of these patterns may lead to the following: 1) Three patterns in the GCM resemble each other; 2) Similarly, the three patterns in the TN model without Reynolds terms (no $\langle Re \rangle$) resemble each other, and so do the three patterns in the TN model with Reynolds terms; and 3) Reynolds terms do not give a particularly large effect to the geopotential height patterns.

To summarize this section, *similar patterns in the extratropics are obtained in three different heating cases by the TN anomaly model, agreeing with the total GCM solutions; the patterns bear some resemblance to the PNA patterns; the amplitudes of the TN model solutions tend to be substantially larger than those of the SL models.*

This experiment suggests that the discrepancy between Step 3 and Step 2 could be ascribed to the effect of transient eddies. In other words, in order to reproduce the PNA pattern, not only is the teleconnection wave train from the equatorial heat source necessary, but also secondarily induced stationary disturbances (the SWB) and transient eddies are also needed.

This finding is by no means new. For example, Simmons (1982) reported that in his numerical experiments, using both the linear and nonlinear time-dependent barotropic model, "the signature of PNA recur again and again". There have been recent studies (for example, Hayashi and Golder 1985; Itoh 1983; Kok and Opsteegh 1985; Nigam et al. 1986), suggesting that quantitatively the nonlinearities due to transient eddies contribute appreciably to the formation of

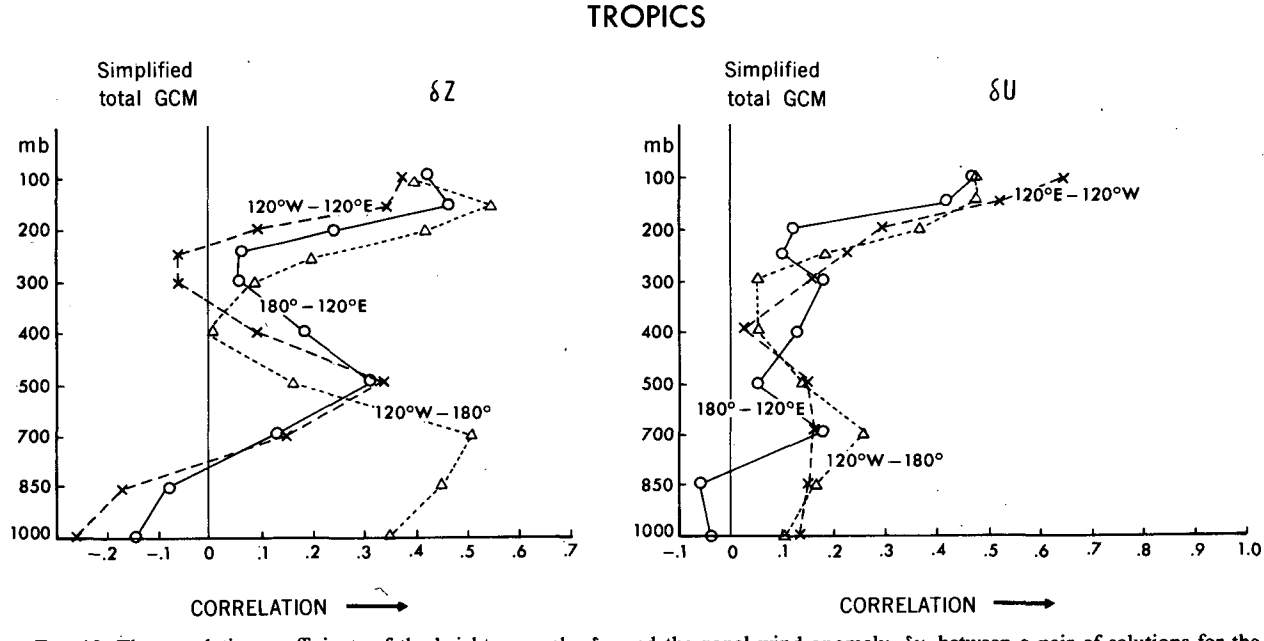

FIG. 10. The correlation coefficients of the height anomaly, δz, and the zonal wind anomaly, δu, between a pair of solutions for the simplified total GCM for different heatings. The abscissa is the coefficient value, and the ordinate is the model's vertical level (mb). The verification domain is the tropics for the latitudinal belt between 25°N and 25°S, and see the text for the longitudinal sector.

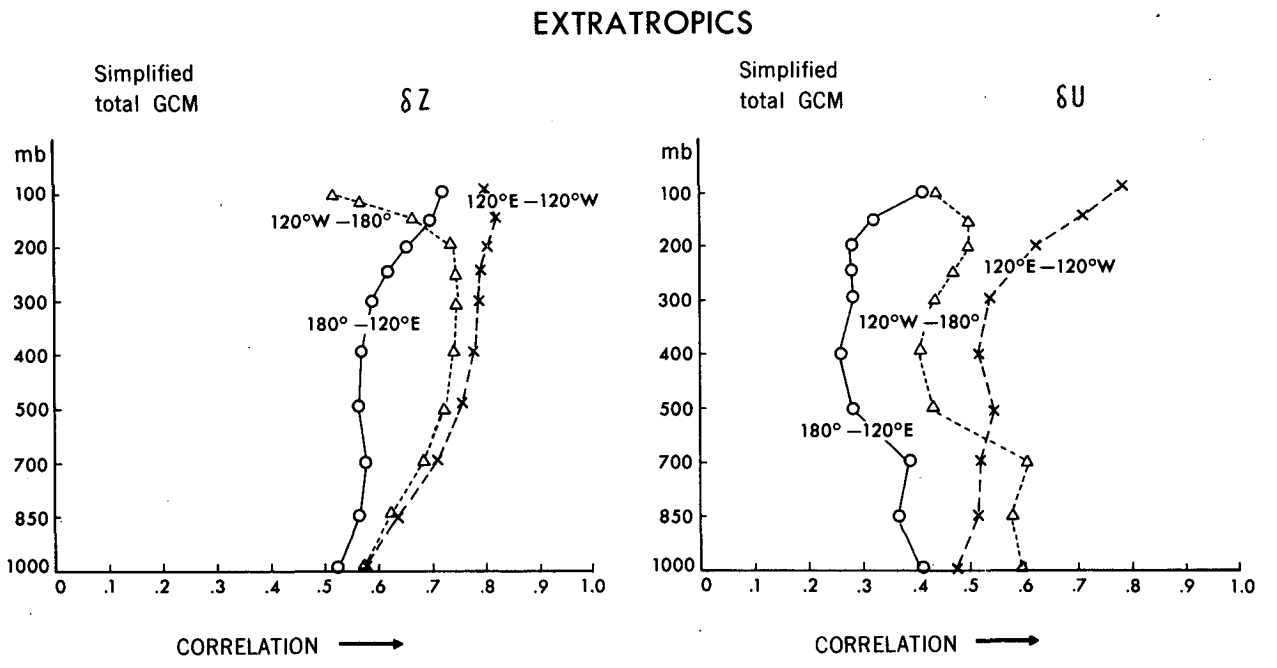

FIG. 11. As in Fig. 10 except for an extratropical verification domain, between 90° and 25°N.

blocking highs. Prior to these studies, Youngblut and Sasamori (1980) and Opsteegh and Vernekar (1982) reached the conclusion, in their analysis of the statistical effect of stationary and transient eddies, that monthly mean geopotential height patterns are significantly affected by transient eddies. A similar relation was pointed out even earlier by Holopainen (1978) in his diagnostic analysis of observational data.

One of the reasons why transient eddies have not received proper attention in the past is that the contribution of this effect to the vorticity budget, for example, is not large as compared with the contributions of other terms, such as the divergence and the horizontal advection of vorticity. Kang and Held (1986) mentioned that the transient eddy term (for summer) is one-fifth of other terms, although it is comparable

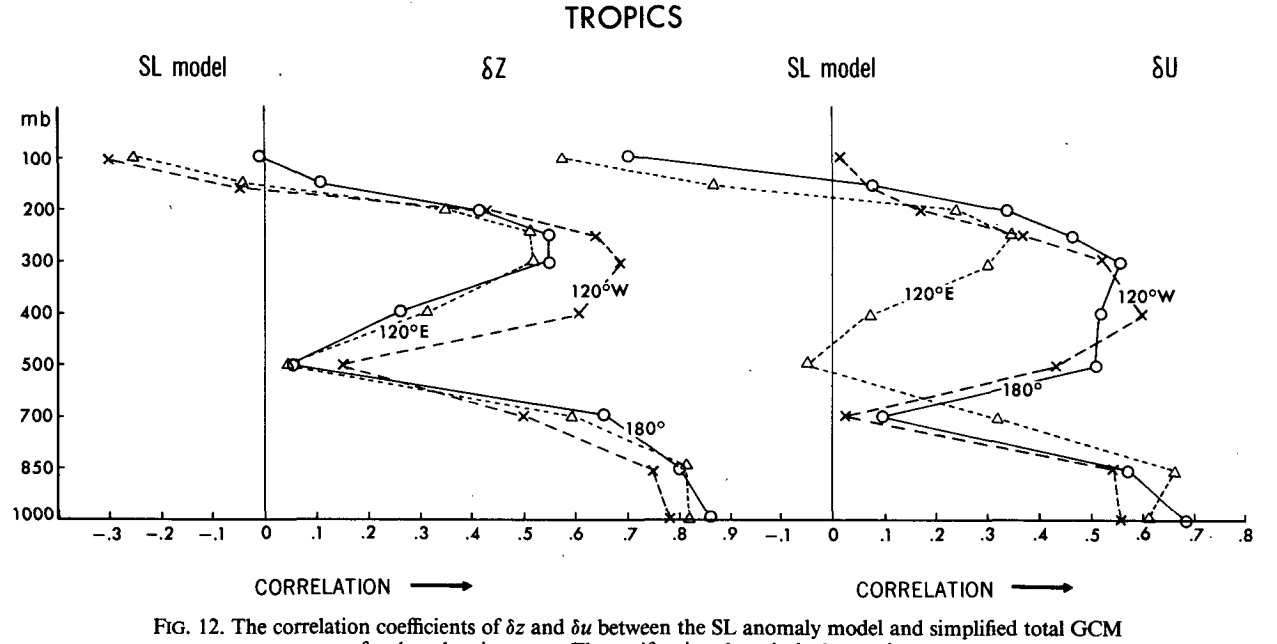

FIG. 12. The correlation coefficients of δz and δu between the SL anomaly model and simplified total GCM for three heating cases. The verification domain is the tropics.

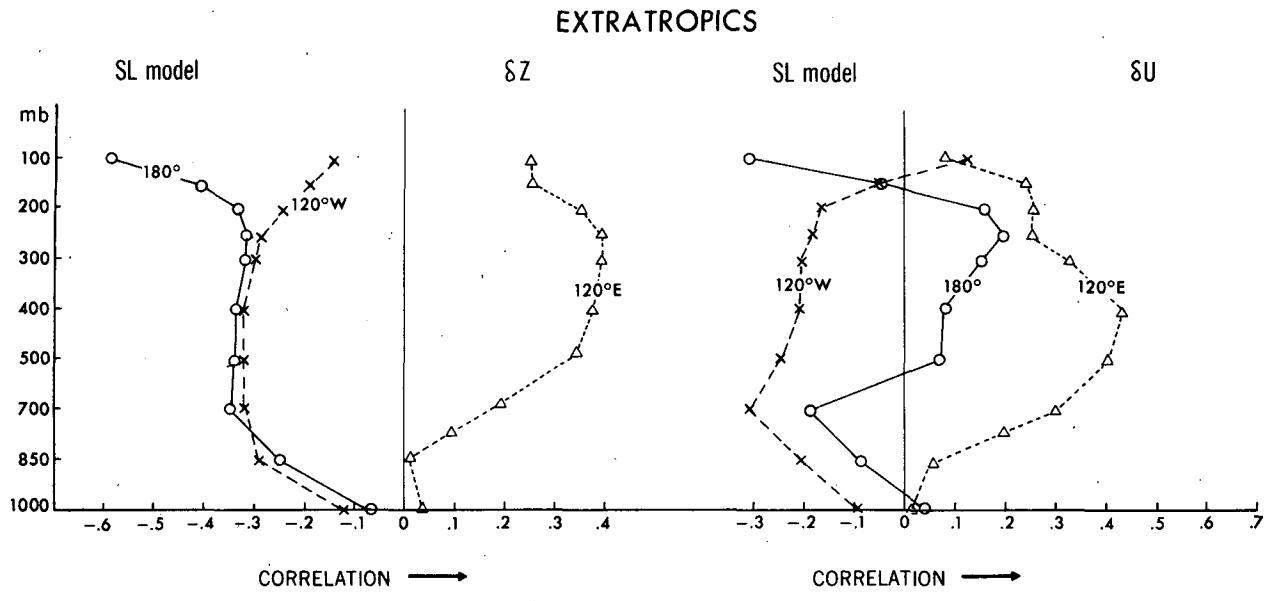

FIG. 13. As in Fig. 12 except the verification domain is for the extratropics.

in certain regions of the globe. Besides, the effect of nonlinearity is included in the vorticity budget in a complicated way. The divergence term in the vorticity equation is, in large part, the implicit result of transient eddies.

The SL model does not seem to be able to obtain good simulations of the GCM monthly anomaly. In particular the PNA-like wavy structures and blocking ridges are misrepresented by the SL model. This indicates that processes left out of the SL model are required to improve the simulation of the GCM anomalies on a monthly time scale. The TN model seems to give some positive indications in this direction. The nonlinear evolution of the SL waves seems to turn them closer to the original GCM anomalies. It is encouraging that this positive result can be achieved in such a preliminary and schematic model as the TN. However, more work is needed to understand the physical mechanisms at work in the TN and put this result on firmer ground. In most past studies, the transient eddies are specified as an external forcing. A unique aspect of the TN is that the transient eddies are treated as the product of the internal dynamics.

9. Conclusions

Anomaly models are constructed based on a spectral GCM of R15L9 resolution. In particular, the SL anomaly model is formulated and solved by a matrix method, using the Krylov technique. This paper, based on the numerical studies with the SL and the TN anomaly models, concludes the following:

TABLE 3. PNA indices (×100).

	120°E	180°	120°W
SL Friction A	22	−14	−11
TN Case I	33	−16	−6
TN Case II	21	−4	10

(i) In contrast to the perturbation model, which uses a zonal, symmetric basic state, the SL anomaly model can handle a zonally varying basic state. The numerical results show that the model's far-field response to equatorial heating is amplified and revitalized in the midlatitude jet region. The resulting anomaly pattern is more complex, and stronger, extending over a larger portion of the hemisphere, than in the zonally symmetric case. These results are in agreement with Navarra (1985).

(ii) However, the SL anomaly model alone cannot account for the anomaly patterns in the extratropics, which are obtained by the full time-dependent nonlinear GCM.

(iii) A better simulation of the anomalies in the Pacific/North American sector can be obtained by allowing a nonlinear time evolution of the SL solution with the TN model. Though the TN result must be regarded as preliminary, the TN model definitely warrants more investigation to sharpen the understanding of the finite amplitude modifications of anomaly waves.

(iv) In the case of January 1983, the observed anomaly patterns both in the near- and far-fields are simulated with considerable skill by the SL anomaly model. But this must be fortuitous, because the PNA patterns are determined, in general, by both the tropical heating and transient eddy effect.

(v) The SL anomaly model is not sufficient for use in long-range forecasting. The TN anomaly model might be usable for this purpose.

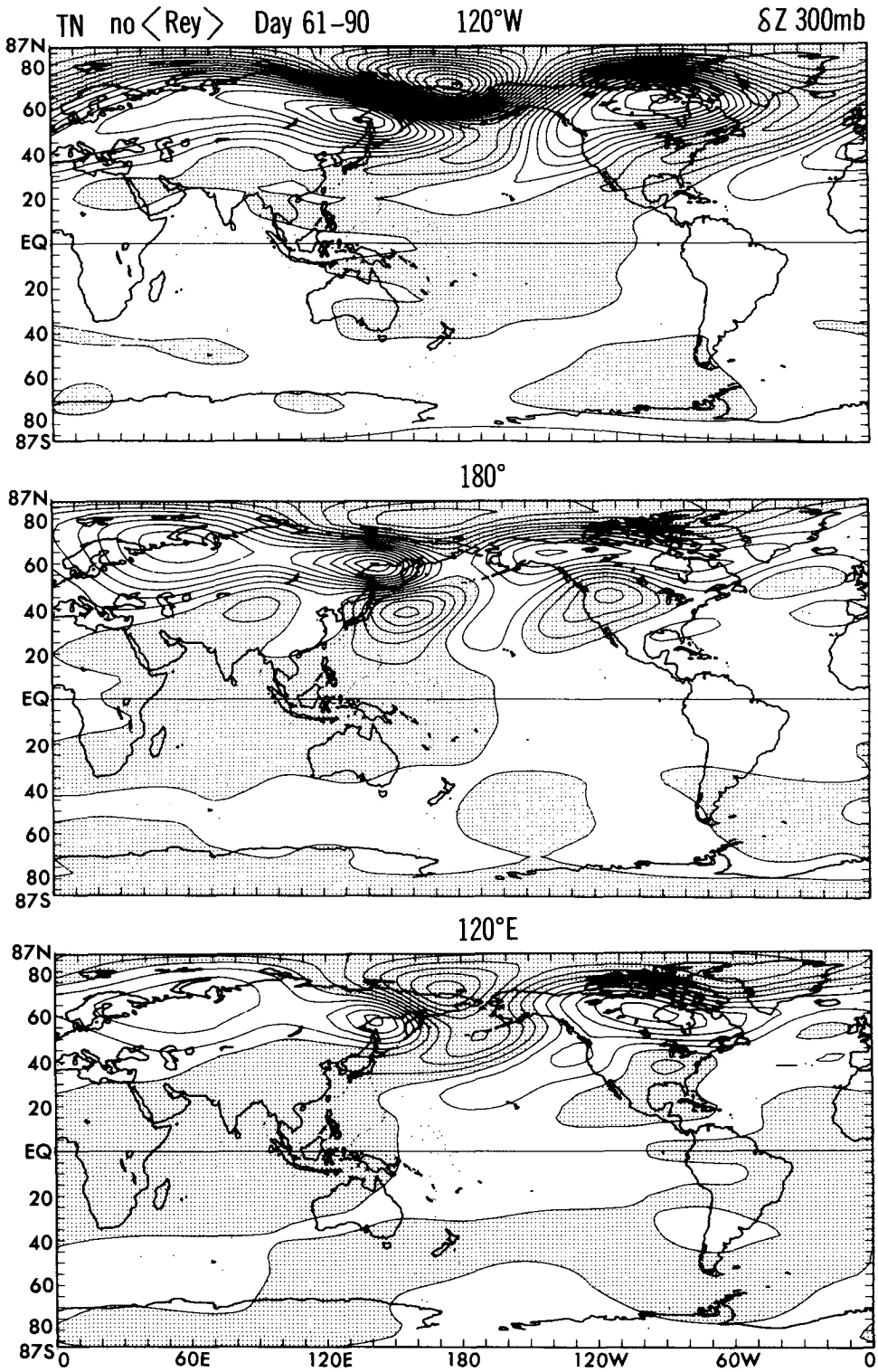

FIG. 14. The 300 mb geopotential height anomalies, as revealed in the monthly averaged patterns from day 61 to 90 of the TN anomaly model with the nodes of the equatorial heat source at the longitudes of 120°W (upper), 180° (middle), and 120°E (lower). Contour interval is 200 m. Negative anomalies are shaded.

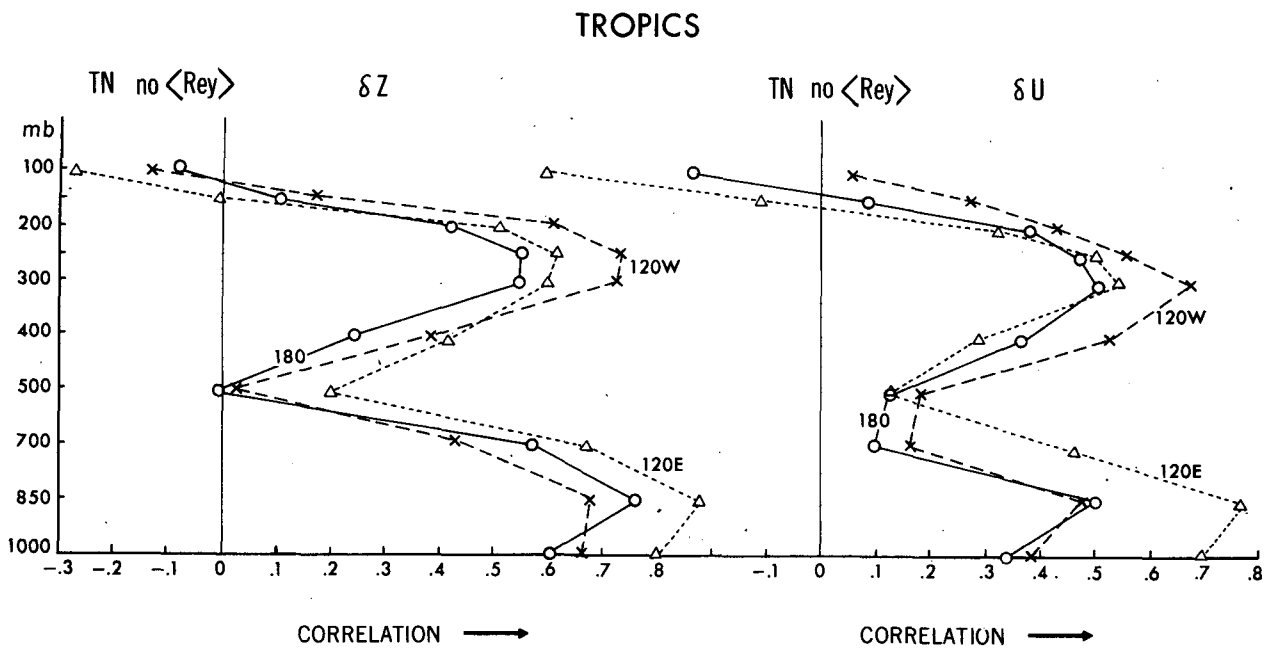

FIG. 15. The correlation coefficients of δz and δu between the TN anomaly model and simplified total GCM for three heating cases. The verification domain is the tropics.

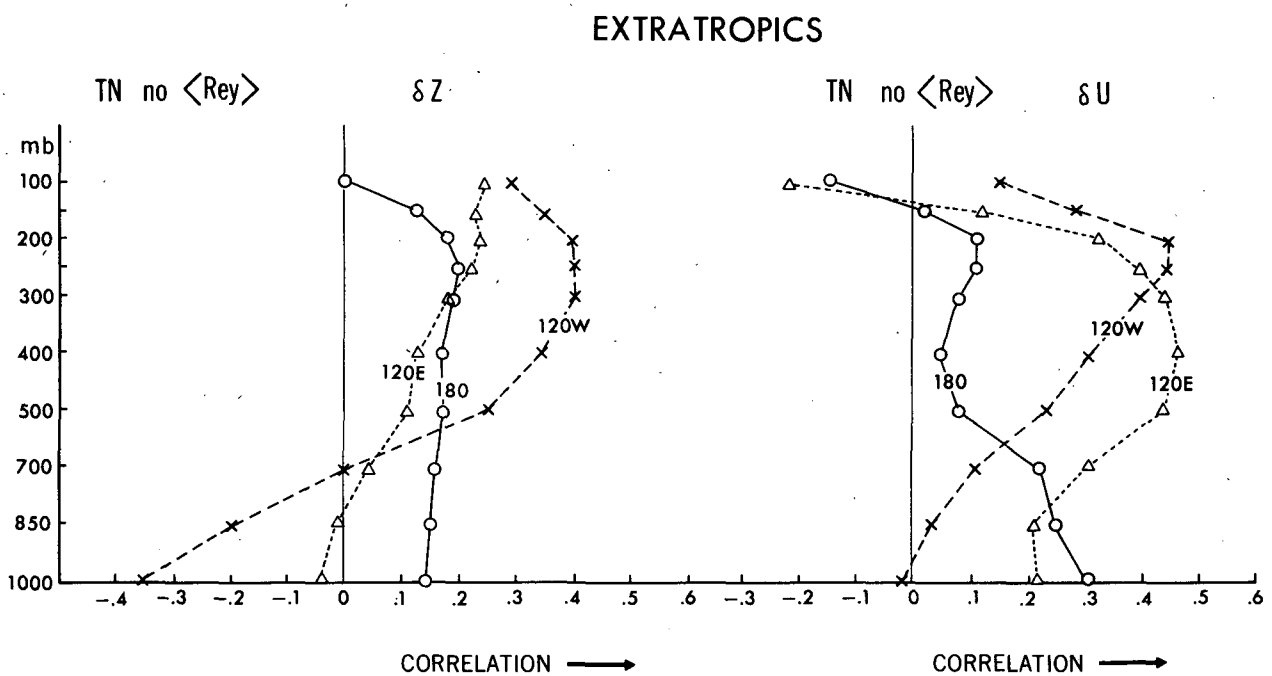

FIG. 16. As in Fig. 15 except for the verification domain of the extratropics.

However, the study with the TN anomaly model in this paper is preliminary, and it needs more refinement and critical assessment.

Acknowledgments. We wish to thank Professor J. P. Chao, Drs. Y. Hayashi, I. Held, N. C. Lau, G. Branstator, and the reviewers for the helpful discussions.

We are also indebted to W. Stern and J. Ploshay, for correcting our grammar, P. Tunison and his group for drafting, J. Connor for photographing, and W. Marshall for typing.

REFERENCES

Arkin, P., 1984: An examination of the Southern Oscillation in the upper tropospheric tropical and subtropical wind field. Ph.D. thesis, University of Maryland, 240 pp.

Blackmon, M. L., J. E. Geisler and E. J. Pitcher, 1983: A general circulation model study of January climate anomaly patterns associated with interannual variation of equatorial Pacific sea-surface temperatures. *J. Atmos. Sci.*, **40**, 1410–1425.

Branstator, G. W., 1983: Horizontal energy propagation in a barotropic atmosphere with meridional and zonal structure. *J. Atmos. Sci.*, **40**, 1689–1708.

——, 1985: Analysis of general circulation model sea-surface temperature anomaly simulations using a linear model. Part I: Forced solutions. *J. Atmos. Sci.*, **42**, 2225–2241.

Chao, J. P., Y. F. Guo and R. N. Xin, 1982: A theory and method of long-range numerical weather forecasts. *J. Meteor. Soc. Japan*, **60**, 282–291.

Crutcher, H. L. and J. M. Meserve, 1970: *Selected Level Heights Temperatures and Dew Points for the Northern Hemisphere.* NAVAIR, Atlas 50-IC-52 Naval Operations. U.S. Govt. Printing Office, Washington, DC, 29 pp.

Cubasch, U., 1985: The mean response of the ECMWF global model to the El Nino anomaly in extended range experiments. *Atmos. Ocean*, **23**, 43–66.

Egger, J., 1977: On the linear theory of the atmospheric response to sea surface temperature anomalies. *J. Atmos. Sci.*, **34**, 603–614.

Frederiksen, J. S., 1979: The effect of long planetary waves on the regions of cyclogenesis: Linear theory. *J. Atmos. Sci.*, **36**, 195–204.

——, 1982: A unified three-dimensional instability theory of the onset of blocking and cyclogenesis. *J. Atmos. Sci.*, **39**, 969–982.

——, 1983: A unified three-dimensional instability theory of the onset of blocking a cyclogenesis II: Teleconnection patterns. *J. Atmos. Sci.*, **40**, 2593–2609.

——, 1983: Distrubances and eddy fluxes in northern hemisphere flows: Instability of three-dimensional January and July flows. *J. Atmos. Sci.*, **40**, 836–855.

Geisler, J. E., M. L. Blackman, G. T. Bates and S. Munoz, 1985: Sensitivity of January climate response to the magnitude and position of equatorial Pacific sea surface temperature anomalies. *J. Atmos. Sci.*, **42**, 1037–1049.

Gill, A. E., 1980: Some simple solutions for heat-induced tropical circulation. *Quart. J. Roy. Meteor. Soc.*, **106**, 447–462.

Gordon, C. T., and W. F. Stern, 1982: A description of the GFDL global spectral model. *Mon. Wea. Rev.*, **110**, 625–644.

Grose, W. L. and B. J. Hoskins, 1979: On the influence of orography on large-scale atmospheric flow. *J. Atmos. Sci.*, **36**, 223–234.

——, W. T. Blakshear and R. E. Turner, 1984: The response of a linear, time-dependent, baroclinic model of the atmosphere to tropical thermal forcing. *Quart. J. Roy. Meteor. Soc.*, **110**, 981–1002.

Group of Long-Range Numerical Weather Forecasting, 1977: On the physical basis of a model of long-range numerical weather forecasting. *Sci. Sinica*, **20**, 377–390.

——, 1979: A filtering method for long-range numerical weather forecasting. *Sci. Sinica*, **22**, 661–674.

Hayashi, Y., and D. G. Golder, 1985: Nonlinear energy transfer between stationary and transient waves simulated by a GFDL spectral general circulation model. *J. Atmos. Sci.*, **42**, 1339–1344.

Held, I. M., 1983: Stationary and quasi-stationary eddies in the extratropical troposphere: Theory. *Dynamics of the Extratropical Troposphere*, B. J. Hoskins, and R. P. Pearce, Eds., Academic Press, 390 pp.

——, R. L. Panetta and R. Pierrehumbert, 1984: Stationary external Rossby waves in vertical shear. *J. Atmos. Sci.*, **42**, 865–883.

Hollingsworth, A., K. Arpe, M. Tiedtke, M. Capaldo and H. Savijarvi, 1980: The performance of a medium-range forecast model in winter-impact of physical parameterization. *Mon Wea. Rev.*, **108**, 1736–1773.

Holopainen, E. O., 1978: On the dynamic forcing of the long-term mean flow by the large-scale Reynolds' stresses in the atmosphere. *J. Atmos. Sci.*, **35**, 1596–1604.

Horel, J. D., and J. M. Wallace, 1981: Planetary-scale atmospheric phenomena associated with the interannual variability of sea surface temperature in the equatorial Pacific. *Mon. Wea. Rev.*, **109**, 813–829.

Hoskins, B. J., 1983: Dynamical processes in the atmosphere and the use of models. *Quart. J. Roy. Meteor. Soc.*, **109**, 1–21.

——, and D. J. Karoly, 1981: The steady linear response of a spherical atmosphere to thermal and orographic forcing. *J. Atmos. Sci.*, **38**, 1179–1196.

Itoh, H., 1983: An observational study on the amplification of planetary waves in the troposphere. *J. Meteor. Soc. Japan*, **61**, 568–589.

Kang, I. S., and I. M. Held, 1986: Linear and nonlinear diagnostic models of stationary eddies in the upper troposphere during Northern summer. *J. Atmos. Sci.*, **43**, 3045–3057.

Kasahara, A, and P. L. Da Silva Dias, 1986: Response of planetary waves to stationary tropical heating in a global atmosphere with meridional and vertical shear. *J. Atmos. Sci.*, **43**, 1893–1911.

Keshavamurty, R. N., 1982: Response of the atmosphere to sea-surface temperature anomalies over the equatorial Pacific and the teleconnections of the Southern Oscillation. *J. Atmos. Sci.*, **39**, 1241–1259.

Kinter, J. L., 1983: Barotropic studies of stationary extratropical anomalies in the troposphere. Ph.D. thesis, Princeton University,

Kok, C. J., and J. D. Opsteegh, 1985: Possible causes of anomalies in seasonal mean circulation patterns during the 1982–1983 El Nino event. *J. Atmos. Sci.*, **42**, 677–694.

Lau, K. M., and H. Lim, 1984: On the dynamics of equatorial forcing of climate teleconnections. *J. Atmos. Sci.*, **41**, 161–176.

Lim, H., and C. P. Chang, 1983: Dynamics of teleconnections and Walker circulations forced by equatorial heating. *J. Atmos. Sci.*, **40**, 1897–1915.

Matsuno, T., 1986: Quasi-geostrophic motions in the equatorial area. *J. Meteor. Soc. Japan*, **44**, 25–43.

Miyakoda, K., and J. P. Chao, 1982: Essay on dynamical long-range forecasts of atmospheric circulation. *J. Meteor. Soc. Japan*, **60**, 292–307.

——, J. Sirutis and J. J. Ploshay, 1986: One-month forecast experiments—without anomaly boundary forcings. *Mon. Wea. Rev.*, **114**, 2363–2401.

Monin, A. S., 1972: *Weather Forecasting as a Problem in Physics.* MIT Press, 199 pp.

Navarra, A., 1985: Anomaly general circulation models. Ph.D. thesis, Princeton University, 202 pp.

——, 1987: An application of the Arnoldi's method to a geophysical fluid dynamics problem. *J. Comput. Phys.*, **69**, 143–162.

Nigam, S., 1983: On the structure and forcing of tropospheric stationary waves. Ph.D. thesis, Princeton University, 203 pp.

——, I. M. Held and S. W. Lyons, 1986: Linear simulation of the stationary eddies in a GCM. Part I: The "no-mountain" model. *J. Atmos. Sci.*, **43**, 2944–2961.

Opsteegh, J. D., and H. M. van den Dool, 1980: Seasonal differences in the stationary response of a linearized primitive equation model: Prospects for long-range forecasting. *J. Atmos. Sci.*, **37**, 2169–2185.

——, and A. D. Vernekar, 1982: A simulation of the January standing wave pattern including the effects of transient eddies. *J. Atmos. Sci.*, **39**, 734–744.

Saad, V., 1981: Krylov subspace methods for solving large unsymmetric linear systems. *Math. Comput.*, **37**, 105–126.

Shukla, J., and J. M. Wallace, 1983: Numerical simulation of the

atmospheric response to equatorial Pacific sea-surface temperature anomalies. *J. Atmos. Sci.*, **40,** 1613–1630.

Simmons, A. J., 1982: The forcing of stationary wave motion by tropical heating. *Quart. J. Roy. Meteor. Soc.*, **108,** 503–534.

——, J. M. Wallace and G. W. Branstator, 1983: Barotropic wave propagation and instability, and atmospheric teleconnection patterns. *J. Atmos. Sci.*, **40,** 1363–1392.

van Loon, H., and J. C. Rogers, 1981: The Southern Oscillation, Part II: Associations with changes in the middle troposphere in the northern winter. *Mon. Wea. Rev.*, **109,** 1163–1168.

Wallace, J. M., and D. S. Gutzler, 1981: Teleconnection in the geopotential height field during the northern hemisphere winter. *Mon. Wea. Rev.*, **109,** 785–812.

Webster, P. J., 1972: Response of the tropical atmosphere to local steady heating. *Mon. Wea. Rev.*, **100,** 518–540.

——, 1982: Seasonality in the local and remote atmospheric response to sea-surface temperature anomalies. *J. Atmos. Sci.*, **39,** 41–52.

——, and J. R. Holton, 1982: Cross equatorial response to middle latitude forcing in a zonally varying basic state. *J. Atmos. Sci.*, **39,** 722–733.

Yanai, M., S. Esbensen and J-H Chu, 1973: Determination of bulk properties of tropical cloud clusters from large-scale heat and moisture budgets. *J. Atmos. Sci.*, **30,** 611–627.

Youngblut, C., and T. Sasamori, 1980: The nonlinear effects of transient and stationary eddies on the winter mean circulation. Part I: Diagnostic analysis. *J. Atmos. Sci.*, **37,** 1944–1957.